ISTANBUL TECHNICAL UNIVERSITY ★ ENERGY INSTITUTE

**INVESTIGATION OF ISTANBUL'S NEOLITHIC AGE ANIMAL FINDINGS
BY NEUTRON ACTIVATION ANALYSIS**

M.Sc. THESIS

Ayşe Tuba ÖNGÜL

**Nuclear Researches Division
Radiation Science and Technology Programme**

JANUARY 2015

ISTANBUL TECHNICAL UNIVERSITY ★ ENERGY INSTITUTE

INVESTIGATION OF ISTANBUL'S NEOLITHIC AGE ANIMAL FINDINGS BY NEUTRON ACTIVATION ANALYSIS

M.Sc. THESIS

Ayşe Tuba ÖNGÜL
(302111001)

Nuclear Researches Division
Radiation Science and Technology Programme

Thesis Advisor: Assist. Prof. Dr. Sevilay HACIYAKUPOĞLU

JANUARY 2015

Ayşe Tuba Öngül, a **M.Sc.** student of ITU **Institute of Energy** student ID **302111001**, successfully defended the **thesis** entitled "**INVESTIGATION OF ISTANBUL'S NEOLITHIC AGE ANIMAL FINDINGS BY NEUTRON ACTIVATION ANALYSIS**", which she prepared after fulfilling the requirements specified in the associated legislations, before the jury whose signatures are below.

Thesis Advisor :   **Assist. Prof. Dr. Sevilay HACIYAKUPOĞLU**   ....
İstanbul Technical University

Jury Members :   **Prof. Dr. Sema AKYIL ERENTÜRK**   ....
İstanbul Technical University

Prof. Dr. Murat BELİVERMİŞ   ....
Istanbul University

Date of Submission : 17 December 2014
Date of Defense :   20 January 2015

I dedicate this thesis to my parents, Zuhal and Metin ÖNGÜL. I hope that this achievement will complete the dream that you had for me all those many years ago when you chose to give me the best education you could. And to my dear fiancee Mustafa DURAN, for his unlimited patience and support.

FOREWORD

TABLE OF CONTENTS

x

ABBREVIATIONS

A.D.	**:** Anno Domini (After Christ)
BNL	**:** Brookhaven National Laboratory
eV	**:** Electron Volt
IAM	**:** İstanbul Archaeology Museum
INAA	**:** Instrumental Neutron Activation Analysis
keV	**:** Kiloelectron Volt
LBL	**:** Lawrence Berkeley Laboratory
N/D	**:** Not defined
REE	**:** Rare Earth Elements
SOM	**:** Sea of Marmara

LIST OF TABLES

LIST OF FIGURES

INVESTIGATION OF ISTANBUL'S NEOLITHIC AGE ANIMAL FINDINGS BY NEUTRON ACTIVATION ANALYSIS

SUMMARY

In the study, the shells of Gastropods, *Mytilus galloprovincialis*, *Acanthocardia spinosa*, *Ostrea edulis*, several fish vertebras as well as a tortoise shell were analyzed by Neutron Activation Analysis. Results were compared to those from the literature to contribute some subjects such as Istanbul's oldest animals lived in Neolithic age by evaluation of the results. Findings were collected from various depths on Marmaray Site from Marmaray-Metro Project Archaeological Excavations at Yenikapı, Istanbul. Neutron Activation Analysis technique was applied by irradiation of samples at the TRIGA Mark II Research Reactor of the Atominstitut of Vienna Technical University. In this frame concentrations of Na, K, Sc, Cr, Fe, Co, Ni, Zn, As, Rb, Sr, Zr, Sb, Cs, Ba, La, Ce, Nd, Sm, Eu, Tb, Yb, Lu, Hf, Ta, W, Th and U elements were determined.

The distribution of the elements in the shells was categorized into three groups. Of these, first 7 elements (Na, K, Fe, Co, Cr, Ni, and Zn) were grouped together because of their contribution to living organisms. Their average concentrations changes from 0,243 to 11,33 mg·kg^{-1}. Second ten elements (Sc, As, Rb, Sr, Zr, Sb, Cs, Ba, Hf, and Ta) are not essential to living organisms, nevertheless may provide additional information regarding e.g. pollution of the sea with further discussion. Their concentrations are between 0,016 and 3,142 mg·kg^{-1}. The remaining ten elements consists from Lanthanides and Actinides (La, Ce, Nd, Sm, Eu, Tb, Yb, Lu, Th and U) which often called *"Rare Earth Elements (REE's)"* are the most commonly investigated elements with NAA. Their average concentration varies between 0,078 and 5,523 mg·kg^{-1} throughout species. The main contribution of Zn and U comes from fish bones and tortoise shell in accordance with the differences in chemical composition between shells and bones of marine animals.

The characteristics of the 27 elements were studied separately in samples. It is known that, in mollusk taxonomy, the elements have unique values. In other words, element concentrations in various mollusk shells depend mainly on the taxonomic characteristics of mollusks. In different bionomic environments, various element distributions of the same species are attributed to the different geochemical characters of the each environment. Considering that the organisms are the most active and deterministic factors of the environment, data obtained in this study will serve as a database for future research.

ISTANBUL NEOLİTİK ÇAĞ CANLILARININ NÖTRON AKTİVASYON ANALİZİ İLE INCELENMESİ

ÖZET

Nötron Aktivasyon Analizi, ister bilimsel ister teknik açıdan olsun, neredeyse akla gelebilecek her alandaki örneklerde farklı miktarlardaki elementlerin (çok, az ve eser), hem nicel hem de nitel analizlerinde uygulanılabilen hassas analitik bir tekniktir. Örnek içinde bulunan kimyasal elementlerin nükleer aktivasyon yöntemi ile radyoaktif hale getirilmesi prensibine dayanan bir kimyasal analiz yöntemidir. Bu yöntemde elementler nötronlarla çarpıştırılarak radyoaktif hale getirildikten sonra, uygun bir radyasyon algılama sistemi ile ölçülürler. Bombardımanda nötronlar kullanıldığında yöntem nötron aktivasyon analizi (NAA) olarak adlandırılmaktadır. Nötron bombardımanında, birim alandan birim zamanda geçen nötron sayısının çok fazla olduğu reaktörler, bilinen en yaygın nötron kaynaklarıdır.

Analizi yapılacak malzemeye belirli bir süre düzgün ve kararlı bir nötron akısı uygulandığında, nötronlar kinetik enerjisinin bir kısmını çekirdeğe ileterek saçılırlar veya tüm enerjisini çekirdeğe ileterek çekirdek içinde yutulurlar. Bu durumdaki çekirdekler fotonlar veya yüklü parçacıklar yayımlayarak kararlı hale geri dönerler. Malzemenin içerdiği elementlerin kararlı izotoplardan nötron yutanlar, yeni ve genellikle uyarılmış bir izotopa dönüşürler. Bu durumdaki çekirdekler 10-12 saniye civarında çeşitli enerjilerde karakteristik gama fotonları salarak kararlı duruma geçerler ki, bu gama ışınları ölçülmez, ya da kararlı izotop oluşabilir. Bu durumda da gama radyasyonu ve ölçme söz konusu değildir, ya da oluşan izotop, algılanabilir bir yarı ömürle β bozumunu yaparak yeni bir elemente dönüşürken γ-ışını verir. Bu ışınlar karakteristik enerji değerine sahip olup, o izotopun kimliğini belirler. Bu γ-ışınlarının enerjileri saptanarak, onları doğuran elementlerin varlığı nitelik olarak ya da şiddetleri ölçülerek, nicelikleri belirlenebilir.

Bu yöntemin uygulanmasında nüklitin tesir kesiti, nötron akısı, nötron kaynağı, radyonüklit oluşumu ve bozunumu, sayım teknikleri, kimyasal ayırma gereksinimi, sistematik hatalar ve örnekleme gibi konular detaylı olarak değerlendirilmelidir. Nötron aktivasyon analizinin uygulanabilmesi için ilgilenilen elementin nükleer reaksiyonlar gerçekleştiğinde yeterli miktarda radyoaktif izotop verebilmesi gereklidir. Bu nedenle nükleer reaksiyonun gerçekleşme olasılığı (tesir kesiti), hedef nüklitin izotopik bolluğu ve oluşan radyoizotopun yarı ömrünün yayımlanan radyoaktivitenin ölçümüne yetecek kadar uzun olması gerekmektedir. Özellikle matriste veya diğer safsızlıklarda meydana gelebilecek radyasyon nedeniyle oluşabilecek girişimlerin anlaşılabilmesi ve giderilebilmesi için meydana gelen radyasyonun tipi ve enerjisi de bilinmelidir.

Bu yöntemin bazı avantajları hassas, hızlı, ekonomik, kolay ve güvenilir bir yöntem olmasıdır. Ayrıca genellikle, ışınlanan malzemede herhangi bir tahribat meydana gelmez ve malzemede kimyasal değişim olmaz. Bir diğer özelliği de pek çok elementin nötronlarla nükleer reaksiyona girmesinden dolayı aynı örnekte aynı anda

birden fazla elementin nitel ve nicel analizi yapılabilir. Birçok element ve uygulama için NAA, diğer metotlarla elde edilemeyecek, milyarda bir veya daha yüksek hassaslık gösterir. Ek olarak, doğruluğu ve güvenilirliğinden dolayı NAA, yeni prosedürler geliştirilirken veya diğer metotlar bir öncekiyle uyuşmayan sonuçlar verdiğinde, genelde referans metot olarak da kullanılır. Başlangıçta yarı iletkenler gibi yüksek saflıktaki malzemelerde, eser miktarda safsızlıkların tayininde kullanılan NAA, günümüzde biyolojik bilimler (kan, doku, saç vb.), jeokimya, kriminoloji, arkeoloji, çevre ile ilgili araştırmalar, endüstriyel uygulamalar gibi çeşitli alanlarda kullanılmaktadır. Dünya çapında NAA araştırmaları o kadar yaygındır ki, her yıl yaklaşık 100,000 örneğin analize alındığı tahmin edilmektedir.

2004 yılında Marmaray tüp geçit projesi inşaatı sırasında, İstanbul Arkeoloji Müzeleri ve İstanbul Üniversitesi Sualtı Kültür Kalıntılarını Koruma Anabilim Dalı tarafından başlatılan Yenikapı kazılarında, on binlerce eser ve Neolitik çağa ait kalıntı gün yüzüne çıkmıştır. Geç Osmanlı döneminden başlayarak, erken Osmanlı, Bizans, Roma, klasik ve arkeik dönem arkeoloji katmanlarının her evresinden buluntularla birlikte İstanbul'un 8,500 yıllk süre içinde geçirdiği kültürel, sanatsal ve jeolojik değişim, deniz ticareti, gemi teknolojisi, kent arkeolojisi, arkeo-botanik, sanat tarihi, filoloji ve dendrokronoloji konularında önemli belgelere ulaşılmıştır. Alanın sağladığı geniş tarih aralığı ve zengin geçmişi dolayısıyla çıkarılan örneklerde analiz yapılarak önemli sonuçlara varılabilir.

Bu çalışmada, nükleer bir analiz yöntemi olan NAA yöntemi kullanılarak, deniz canlısı örneklerindeki elementlerin belirlenmesi amaçlanmıştır. Bu kapsamda kullanılan örnekler, İstanbul Arkeoloji Müzeleri Müdürlüğü'nün izniyle Yenikapı Marmaray ve metro kazıları esnasında çıkarılan Neolitik Çağ Dönemine ait olduğu belirlenmiş ve etütlük olarak tanımlanan deniz canlısı buluntularıdır.

Seçilen örnekler, kazı alanında çeşitli derinliklerden toplanmış olan, *Gastropod (Eklembacaklı)*, *Mytilus galloprovincialis (Kara midye)*, *Acanthocardia spinosa*, *Ostrea edulis (İstiridye)*, balık omurgası ve kablumbağa kabuğundan oluşmaktadır.

Element miktarlarının belirlenmesi için Viyana Teknik Üniversitesi, ''*Atominstitut*'' bünyesinde bulunan TRIGA Mark II nükleer araştırma reaktöründe, Nötron Aktivasyon Analizi yöntemi kullanılmıştır. Bu amaçla buluntular önce çeşitli işlemlerden geçirilerek dış kirliliklerden arındırılmıştır. Buluntular daha sonra öğütülüp, belirlenen miktarlarda tartılıp, kuarz ışınlama tüplerine yerleştirilip, kapatılıp reaktörde 30-40 saat sürelerde ışınlanmaya maruz bırakılmışlardır. Işınlanan örneklerle birlikte çeşitli sertifikalı standart malzemeler de paketlenmiştir. Uygulanan çeşitli soğuma ve ölçüm sürelerine göre Na, K, Sc, Cr, Fe, Co, Ni, Zn, As, Rb, Sr, Zr, Sb, Cs, Ba, La, Ce, Nd, Sm, Eu, Tb, Yb, Lu, Hf, Ta, W, Th ve U elementlerine dair veriler elde edilmiştir.

Örneklerdeki element dağılımı, canlı için hayati, hayati olmayan ve periyodik tabloda lantanit ve aktinitler olarak sınıflandırılan eser elementler olmak üzere üç grupta incelenmiştir. Birinci grupta incelenen 7 elementin (Na, K, Fe, Co, Cr, Ni ve Zn) incelenen tüm türler için ortalama konsantrasyonu 0,243-11,33 mg·kg^{-1}; ikinci on elementin (Sc, As, Rb, Sr, Zr, Sb, Cs, Ba, Hf ve Ta), 0,016-3,142 mg·kg^{-1}; geriye kalan on elementin (La, Ce, Nd, Sm, Eu, Tb, Yb, Lu, Th, ve U) ise 0,078-5,523 mg·kg^{-1} olarak bulunmuştur.

Çinko ve uranyum konsantrasyonları, balık omurgaları ve kablumbağa kabuğunun kimyasal yapısıyla doğru orantılı olarak diğer örneklerden yüksek çıkmıştır. Aynı zamanda kemiklerde eser elementlerin birikim davranışları gözlemlenebilmiştir.

Bu çalışma ile Neolitik Çağa ait deniz canlısı örneklerinde NAA ile element konsantrasyonlarının belirlenmesinin, kendi aralarında ve modern literatur ile karşılaştırılarak yorumlanmasının, Istanbul'un binlerce yıl önceki deniz canlılarının özelliklerine ışık tutabileceği ve merak edilen sorulara cevap bulabileceği düşünülmektedir.

1. INTRODUCTION

From the written sources, it has already been known that there was a port in Yenikapı, Istanbul but never been searched before. In 2004, with the Marmaray Tube Tunnel Project, began exploratory archaeological excavations, which have been conducted jointly by the Istanbul Archaeological Museums and the Istanbul University Department of Conservation of Underwater Cultural Heritages. For ten years, findings from excavations uncovered the history of Istanbul from the late Ottoman period back to the early Byzantine period, even to the Neolithic age. It covers a period of 8,500 years of history of Istanbul. Also, relates to the cultural, artistic and geological changes, maritime trade, ship technology, urban archaeology, archaeobotanical, history of art, philology and so on [1].

In an area of 58 thousand square meters in Yenikapi, more than 35,000 archaeological findings have been unearthed to this date including the Harbor of Theodosius, which was built by Theodosius I (379 - 395). It was the first trading port in the city in the Early Byzantine Period and dates some 1,600 years back at a depth between -1 and -6,30 meters [1].

It has been believed according to the findings that the Harbor was the center of the world trade in the 4th century. Also, found, it had become mostly useless due to the alluvium deposited by the stream, but it continued to be used until the 11th century as a shelter by smaller ships and boats. The findings from the excavations shed light on the history of the city of Istanbul. It provided data to track the changes undergone by the Sea of Marmara for the last 10.000 years, with the help of the marine elements layered between architectural remnants from the Neolithic Age [1].

Many disciplines prefer Neutron Activation Analysis (NAA) for the assessment of elements present in samples. From archaeology, biomedicine, environmental monitoring, food, forensic science, geological and inorganic materials, agriculture, industrial applications, even to the quality assurance for determining the purity of semiconductors.

So despite the developments of other analytical techniques, which use physical, chemical and nuclear characteristics. It is still one of the primary method employed in particular fields of science, depending on the purpose [2].

The greatest advantage of it is the fact that the samples do not have to be treated with any chemical treatment, before or after the activation. It makes INAA non-destructive and lower the probability of contamination from laboratory. It can observe trace elements mostly at amounts in microgram to nanogram or even less. Using the high selectivity of gamma-ray spectrometry allows the determination of radionuclides simultaneously. It is usually used as a valuable reference for other analysis methods. Worldwide application of NAA is so widespread; it is estimated that approximately 100,000 samples undergo examination each year [3].

For provenance research, characterising archaeological materials with the application of NAA has been used successfully and increasingly since Robert Oppenheimer recognised it in the autumn of 1954. NAA's results provide information to archaeologists about questions such as sources of raw materials, trading practices, the location of prehistoric production areas and the mobility patterns of ancient peoples.

Marine biogenic carbonates provide environmental records to the media in which they have grown. Trace elements deposited in the marine system can be transferred into the biota and may be affected by chemical and biological processes in the water column, sediments and biota. Data obtained from the investigation can provide indirect evidence of climatological diversity, or reveal unusual temporal changes in elemental uptake possibly related to anthropogenic complexity of the environment [4,5].

The aim of the study was to analyse the archaeological finds by NAA, compare the results to those from the literature, and contribute some subjects such as Istanbul's oldest animals lived in Neolithic Age. By the evaluation of the results and also to evaluate the levels of elemental concentrations, as well as bioaccumulation factors in some of the species collected from the Yenikapı-Marmaray site. In this way, questions may be addressed by the production, distribution and use of organic substances in the ancient world. Most organic materials are subject to microbial, and chemical degradation and thus useful biomarkers are only those that are sufficiently robust to survive long-term deposition, such as shells and bone.

2. NEUTRON ACTIVATION ANALYSIS AND ARCHEOLOGY

NAA is very useful for trace and ultra-trace analysis of samples above all other nuclear analytical techniques. When combined with spectroscopic methods it is an efficient and precise method for multi-element investigation in trace element work.

Two years after Chadwick discovered the neutron in 1932, came the discovery of the induced radioactivity by Irene Joliot and Frederic Curie. In the 1930s, one of the first to use neutrons for producing artificial radioactive isotopes was Enrico Fermi. Following the direction of his research George de Hevesy used it to study the rare earth elements. When Hevesy and Levi found that the samples consists of certain rare earth elements became radioactive after exposed to a source of neutrons, it marked the beginning of neutron activation analysis. Thus in 1936, Hevesy and Levi, released the first publication on the application of neutron activation analysis, which stated, "… The usual chemical methods of analysis fail, as is well known, for most of the rare earth elements and have to be replaced by spectroscopic, X-ray, and magnetic methods. The latter methods can now be supplemented by the application of neutrons to analytical problems by making use of the artificial radioactivity and the high absorbing power of some of the rare earth elements for slow neutrons…." [2].

Boyd was the one who suggested to term the procedure "… the method of radio activation analysis …", Alternatively, "… Activation analysis…". In 1949 Boyd proposed to name the process "… the method of radio activation analysis …", Or, more succinctly, "… activation analysis…" and he discussed the use of the "… Chain-Reacting pile …" as a source of neutrons and an example of an analysis was given.

With the advances in gamma-ray spectrometry and scintillation detectors, technique was further improved as it provided much better radionuclide selectivity. Many applications still needed chemical separations. But with the semiconductor detector's introduction in the beginning of 1960s, selectivity in gamma ray spectrometry was

increased to such an extent that radionuclides could be determined directly in a pool of radioactivities and thus removing the need for chemical separations. It set the start of INAA as an essential form of NAA and improved further by the multichannel pulse height analysers and laboratory computers [2].

INAA has been found useful in many fields of science. The greatest advantage of it is the fact that the samples do not have to be treated with any chemical treatment, before or after the activation. It makes INAA non-destructive and lower the probability of contamination from laboratory. In addition, interference from elements like H, C, N, Si, can be eliminated because they do not produce radioactive products during neutron activation thus ensuring the determination of other activities, clearer.

It can observe trace elements mostly at amounts in microgram to nanogram or even less. Using the high selectivity of gamma-ray spectrometry allows the determination of radionuclides simultaneously. The preparation of the samples is very easy. An amount of it just needs to be weighed and place in a suitable container. The results are not affected by the chemical or physical state of the elements.

Because of its accuracy and precision, it is still one of the primary methods employed by the National Institute of Standards and Technology to certify the concentrations of elements in standard reference materials. It is used for materials which required to be pure to the highest degree, such as semi-conductors, archaeology, agriculture, criminology, geochemistry, environmental monitoring, industrial applications, health, human nutrition and even for art [6].

2.1 Fundamentals of Neutron Activation Analysis

Essentially, Neutron activation is the irradiation of a nucleus with neutrons to produce radioactive species, usually referred to as the radionuclide. The number of radionuclides produced, depend on the number of neutrons, the number of target nuclei, and on the cross section, which defines the probability of activation occurring. If the activation product is radioactive, it will decay with a characteristic half-life. Consequently, the growth of activity during irradiation will depend on the half-life of the product. The energy of the neutrons that are bombarding the nucleus will dictate the type of interaction that occurs and consequently the nature of the

activation product. Therefore, if the nucleus is irradiated in a neutron flux of both slow and fast neutrons, there may be more than one activation product.

Similarly, interferences may occur as the result of the same radionuclide being produced by the activation of different target nuclei.

2.2 Nuclear Reactions

Neutrons can exhibit a broad range of energies. In a thermal nuclear reactor, for example, the neutrons are moderated, and the majorities are thermal or slow neutrons with an average energy of about 0.025 eV. A neutron generator is designed to produce fast neutrons with energy of 14 MeV. The region between thermal and fast neutrons is called the "epithermal region," extending from 0.5 eV to 1 MeV.

The lower cutoff at 0.5 eV is defined by the energy below which neutrons will not pass through 1 mm thick cadmium. Therefore, it is sometimes referred to as the cadmium cutoff.
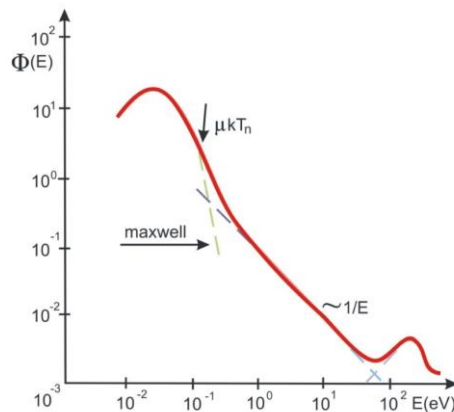
Figure 2.1 : Distribution of neutrons according to their energies in nuclear reactor [7].

A neutron is absorbed by the target nucleus to produce an extremely energetic state of the resulting nucleus containing an additional neutron. The excess energy is immediately lost, usually by emission of a gamma ray, a proton or an alpha particle. The energy of the neutron will affect the nature of the nuclear reaction, which occurs, and consequently the activation product. The primary reaction occurring with thermal neutrons is the so-called (n,γ) reaction:

$$^{27}Al + n \ ----» \ ^{28}Al + \gamma \tag{2.1}$$

In this case, the highly energetic level of the product nucleus is de-excited by emission of a gamma ray, which is called a prompt gamma, since it is emitted immediately after activation. Fast neutrons induce different reactions. The absorption occurs with either the ejection of a proton, in the case of an (n,p) reaction, for example:

$$^{31}P + n \text{ ----» } ^{31}Si + p \tag{2.2}$$

or the production of an alpha particle, as in the case of an (n, α) reaction:

$$^{23}Na + n \text{ ----» } ^{20}F + \alpha \tag{2.3}$$

The gamma rays, protons and alpha particles produced during these reactions are all emitted spontaneously and therefore they are only detected if they are monitored during the activation process. It is possible to see all three typical reactions: (n,γ), (n,p) and (n,α), occurring with one target nucleus, for example in the case of ^{23}Na where not only the (n, α) reaction shown above occurs, but also the (n, y) and the (n,p) reactions:

$$^{23}Na + n \text{ ----» } ^{24}Na + \gamma \tag{2.4}$$

$$^{23}Na + n \text{ ----» } ^{23}Ne + p \tag{2.5}$$

So in a neutron flux consisting of slow and fast neutrons the activation of ^{23}Na will result in the production of ^{24}Na, ^{20}F and ^{23}Ne. These activation products are all radioactive, but the product of a neutron-induced reaction may be a stable, naturally occurring isotope of the particular element.

2.3 Activation With Neutrons

In a neutron-induced reaction, the growth of the product is dependent on the size of the neutron flux. The larger the neutron flux, the greater the rates at which interactions occur:

$$\text{Activation rate} \propto \text{neutron flux } (\phi)$$

The activation rate is also directly proportional to the number of target nuclei present:

$$\text{Activation rate} \propto \text{number of nuclei present (N)}$$

The number of target nuclei present will depend on the isotopic abundance of the particular isotope of interest. For example, aluminum is composed entirely of stable ^{27}Al, and so all the target nuclei will be the same.

However, there may be more than one isotope of an element, such as in the case of calcium where there are six stable isotopes: ^{40}Ca, ^{42}Ca, ^{43}Ca, ^{44}Ca, ^{46}Ca and ^{48}Ca. As an example, ^{48}Ca is only present as 0.185 % of the total. In such cases the number of target nuclei must be corrected for the isotopic abundance (a):

$$N = m\ a\ N_A / M \qquad\qquad (2.6)$$

The number of target nuclei is, therefore, proportional to the mass of element present. Since the growth of the activation product is proportional to the number of target nuclei, it follows that the activation rate is commensurate with the mass of the element:

Activation rate $\propto$ mass of element *(m)*

It is, therefore, possible to deduce the mass of element present from the induced activity. It forms the basis of the neutron activation analysis technique. If the neutron flux remains constant, then the "calibration curve" for an element can be determined by plotting the induced activity against the mass of the element.

The simple relationship is shown in Figure 2.2 for ^{60}Co using the data from the compilation of calculated activities. The activity is given for a 10 d irradiation in a thermal neutron flux of 10^{16} m^{-2} s^{-1}. The slope is equivalent to the specific activity and goes through zero.
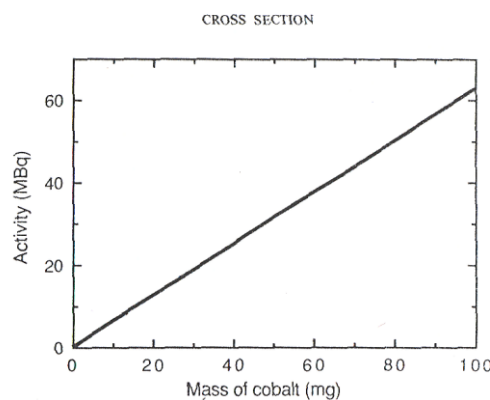
Figure 2.2 : Standardization curve for cobalt, irradiated in a thermal neutron flux of 10^{16} m^{-2} s^{-1} for 10 d, showing the linear relationship between the mass of the element and the induced activity [8].

2.3.1 Cross section

The relationship between activation rate, the number of target nuclei and the neutron flux is expressed by the term "cross section" (σ). The cross section is simply a physical constant:

$$\text{Activation rate} = \sigma \, \Phi \, N \qquad \qquad \textbf{(2.7)}$$

N is the number of target nuclei, in atoms

Φ is the neutron flux, in neutrons $m^{-2} \, s^{-1}$

σ is the cross section, in m^2

activation rate is in events s^{-1}

Substituting:

$$N = m \, a \, N_A \, / \, M \qquad \qquad \textbf{(2.8)}$$

into the expression for activation rate, it becomes:

$$\text{Activation rate} = \sigma \, \Phi \, m \, a \, N_A \, / \, M \qquad \qquad \textbf{(2.9)}$$

Cross sections are usually expressed in barns which are $10^{-24} \, m^2$. As a rough guide, a target nucleus with a cross section in the order of barns will activate well but a cross section of millibarns indicates weak activation. It is important to remember that each stable isotope of the same element will have a different cross section. Consequently, one isotope may have a high cross section and become very active while another isotope of the same element may have a small cross section and be activated to a much smaller extent. It is, therefore, important to consider the cross sections when deciding which target nuclide to use inactivation analysis.

The neutron cross section for a particular nucleus will depend on the energy of the neutron. Many nuclei, particularly of small atomic number absorb thermal neutrons with cross sections that decrease linearly with increasing velocity of the neutron (known as 1/v absorbers). It is usual to refer to thermal cross sections for the absorption of neutrons with an average velocity of 2,200 m s^{-1}. Tables of cross sections are available for activation with neutrons.

In the tables, the cross sections may be expressed in different forms. So, the total cross section given for a particular target will be composed of a number of partial cross sections, dependent on the activation process, including (n,γ), (n,p) and (n,α) reactions. However for most thermal neutron activation the primary process is the (n,γ) reaction involving the neutron radiative capture cross section (σ_γ).

Not all target nuclei are 1/v absorbers, and there are many examples of nuclei that preferentially absorb epithermal neutrons. At these higher energies, the neutron cross section is referred to as the resonance integral and the radiative capture resonance integral (I_γ) is used. Some typical examples are shown in Table 1.1. It can be seen from the cross section values that the lighter elements have thermal cross sections and resonance integrals in the same order. They are the 1/v absorbers.

Table 2.1 : Capture cross sections (σ_γ) and resonance integrals (I_γ) (in barns) for some typical activation targets [8].

Target	σ_γ	I_γ	Target	σ_γ	I_γ
^{23}Na	0.4	0.31	^{63}Cu	4.5	5.0
^{26}Mg	0.038	0.026	^{75}As	4.3	61
^{27}Al	0.23	0.17	^{81}Br	2.4	60
^{37}CI	0.43	0.30	^{109}Ag	91	1400
^{48}Ca	1.09	0.89	^{139}La	8.9	11.8
^{5I}V	4.9	2.7	^{152}Sm	206	2970
^{50}Cr	15.9	7.8	^{152}Eu	9200	3300
^{55}Mn	13.3	14.0	^{186}W	37.9	485
^{58}Fe	1.28	1.7	^{191}Ir	954	3500
^{59}Co	37.2	74	^{197}Au	98.7	1550

On the other hand, the isotopes ^{109}Ag, ^{152}Sm and ^{197}Au have vast resonance integrals compared to the thermal cross sections, indicating that there are strong resonances in the region above the cadmium cutoff energy. In these cases it is important to include the resonance integral term in the calculation of the activation rate:

$$\text{Activation rate} = \sigma_\gamma\, \Phi_{th}\, N \ + \ I_\gamma\, \Phi_{epi}\, N \tag{2.10}$$

Φ_{th} is the thermal neutron flux, Φ_{epi} is the epithermal neutron flux.

9

2.3.2 Decay rate

If the product nuclide in a neutron-induced reaction is stable the number of nuclei produced is easily calculated from the activation equation by multiplying by the length of irradiation, t:

$$\text{Activation rate} = \sigma \, \Phi \, N$$

$$\text{Number of nuclei} = \sigma \, \Phi \, N \, t$$

However, if the product nuclide is radioactive it will have a decay rate which must be taken into account. The radionuclide produced will decay with a characteristic half-life. If there are $N*$ radioactive nuclei, the rate of decay of the nuclei is proportional to N*:

$$\text{Decay rate, } dN*/dt* \propto -N* \qquad (2.11)$$

$$= -\lambda N \qquad (2.12)$$

where λ is the decay constant, which has a characteristic value for each radionuclide. If the equation is integrated between the limits N_0* at time zero, and $N*$ remaining at time t:

$$N* = N_0* \exp(-\lambda t) \qquad (2.13)$$

It is from the above expression that the term half-life is derived since, for if the time for half the nuclei to decay is defined as $t_{1/2}$:

$$N_0* / 2 = N_0* \exp(-\lambda \cdot t_{1/2}) \qquad (2.14)$$

$$t_{1/2} = \ln2/\lambda = 0.693 / \lambda \qquad (2.15)$$

A semilogarithmic plot of the decay rate against time will give a straight line graph with a slope of $-\lambda$. Figure 2.3 shows the plot that would be obtained for ^{56}Mn which has a half-life of 2.58 h. The half-life of the radionuclide can be read directly from the time taken for the decay rate to be reduced by a half.
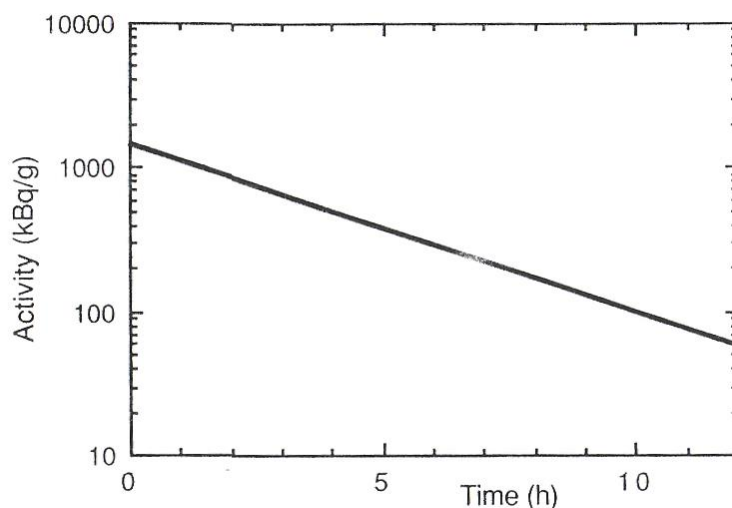
Figure 2.3 : Decay curve for ^{56}Mn ($t_{1/2}$ = 2.58 h), showing the semilogarithmic relationship between length of decay and remaining activity [8].

A table of the half-lives, for some radionuclides commonly measured by neutron activation analysis are given in Table 2.1. Because the half life is characteristic for a particular radionuclide it can be used to identify an unknown species or confirm the identity of the radionuclide being measured.

Product	Half-life	Product	Half-life
^{24}Na	14.57 h	^{64}Cu	12.70 h
^{27}Mg	9.46 min	^{76}As	26.3 h
^{28}Al	2.24 min	^{82}Br	35.3 h
^{38}Cl	37.2 min	^{110}Ag	24.6 s
^{49}Ca	8.72 min	^{140}La	40.3 h
^{52}V	3.75 min	^{153}Sm	46.7 h
^{51}Cr	27.70 d	^{152}Eu	13.3 y
^{56}Mn	2.578 h	^{187}W	23.9 h
^{59}Fe	44.5 d	^{192}Ir	73.8 d
^{60}Co	5.27 y	^{198}Au	2.69 d

Figure 2.4 : Half-life values for typical activation products [8].

2.3.3 Induced activity

If the activation product is radioactive and decays with its characteristic half-life, the radionuclide is being produced at the rate described by the activation equation and decaying with the characteristic half-life. Consequently the growth of the activity is governed by the difference between them: Production rate = Activation rate - Decay rate;

11

$$dN^* /dt = \sigma \, \Phi \, N - \lambda \, N^* \qquad\qquad (2.16)$$

$$N^* = \sigma \, \Phi \, N \, (1 - \exp(-\lambda t)) / \lambda \qquad\qquad (2.17)$$

The activity or disintegration rate (A_0), at the end of the irradiation time t, is then:

$$A_0 = \lambda \, N^* = \sigma \, \Phi \, N \, (1 - \exp(-\lambda t_i)) \qquad\qquad (2.18)$$

Consequently the growth of the induced activity with time is controlled by the half-life of the activation product. This is demonstrated in Figure 2.4, where the growth curve for ^{49}Ca ($t_{1/2}$ = 8.72 min) is plotted. It can be seen that the majority of the activity is produced during the first two half-lives. When the irradiation time is very long the expression for activity becomes close to the maximum possible activity for a particular neutron flux, called the saturation activity (A_s):

$$A_s = \sigma \, \Phi \, N \qquad\qquad (2.19)$$
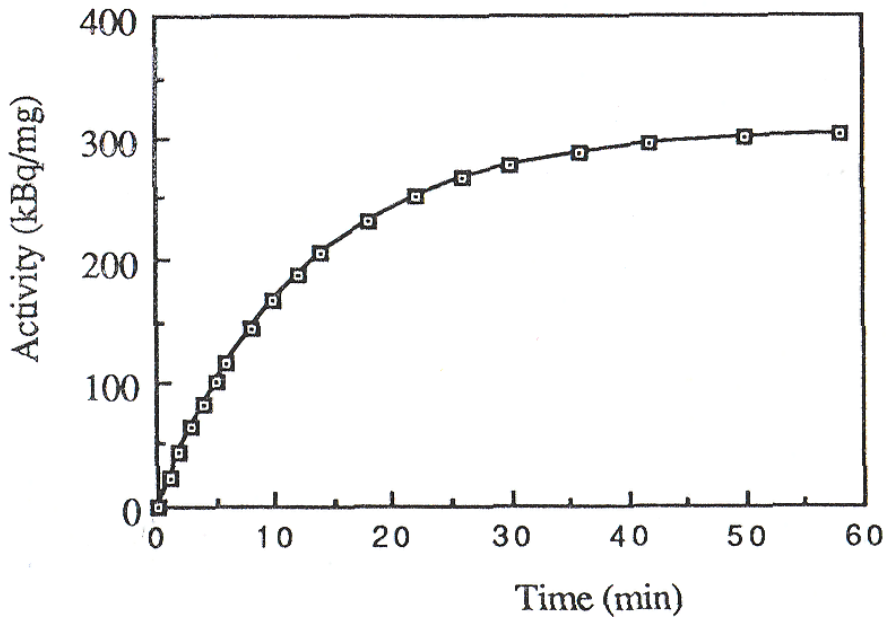
Figure 2.5 : Activation curve for ^{49}Ca ($t_{1/2}$) = 8.72 min) [8].

The saturation activity is independent of the half-life of the activation product and depends only on the value of the neutron flux and neutron cross section. A plot of activity induced in ^{64}Cu for different neutron fluxes in Figure 2.5 shows the growth of activity to saturation and how the saturation activity increases with neutron flux.
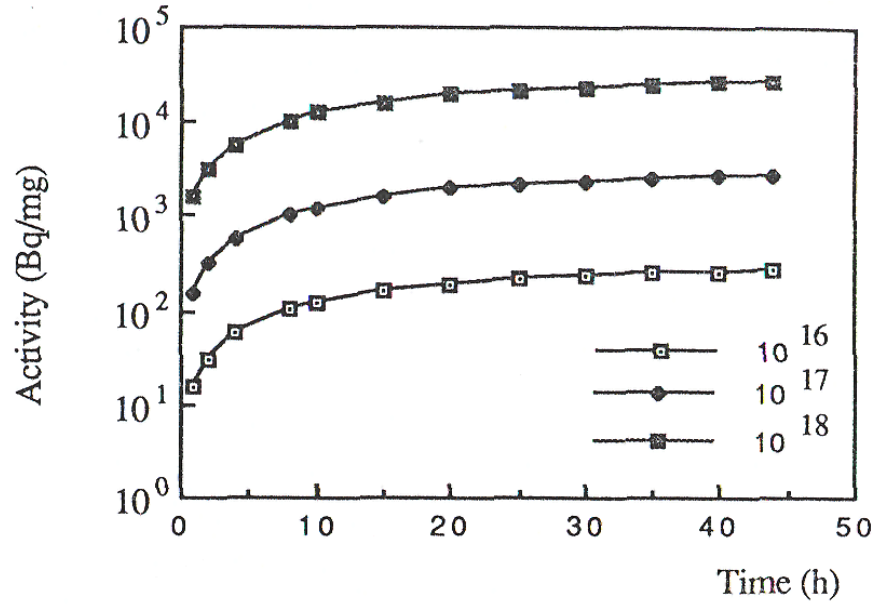
Figure 2.6 : Activation curves for ^{64}Cu ($t_{1/2}$ = 12.70 h), showing the increase in saturation activity with increasing neutron flux, from 10^{16} to 10^{18} n m^{-2} s^{-1} [8].

Unless the activation product is relatively short-lived it is not convenient to allow the growth curve to reach saturation. The usual form of the equation for activity at the end of an irradiation for a time t is:

$$A_0 = \sigma \, \Phi \, N \, (1 - \exp(-\lambda t_i)) \qquad\qquad \textbf{(2.20)}$$

It is possible to calculate the induced specific activity for a particular length of irradiation, knowing the nuclear constants for the nuclide of interest and the neutron flux:

$$A_0 = \sigma \, \Phi \, m \, a \, N_A \, (1 - \exp(-\lambda t_i)) \, / \, M \qquad\qquad \textbf{(2.21)}$$

Usually in neutron activation analysis, the activity of the radionuclide is measured experimentally in a sample to deduce the unknown mass of the element using the activation equation:

$$m = A_0 \, M \, / \, (a \, N_A \, \sigma \, \Phi \, (1 - \exp(-\lambda t_i))) \qquad\qquad \textbf{(2.22)}$$

Corrections must also be made for the decay period t_d before counting:

$$m = A_0 \, M \, / \, (a \, N_A \, \sigma \, \Phi \, (1 - \exp(-\lambda t) \exp(-\lambda t_d)) \qquad\qquad \textbf{(2.23)}$$

13

2.4 Derivation of the measurement equation

The reaction rate R per nucleus capturing a neutron is given by:

$$R = \int_0^\infty \sigma(v)\,\phi'(v)dv = \int_0^\infty \sigma(E)\phi'(E)dE = \int_0^\infty n'(v)v\sigma(v)dv \qquad (2.24)$$

where:

$\sigma(v)$ is the (n,γ) cross section (in cm^2 ; 1 barn (b) $= 10^{-24}\ cm^2$) at neutron velocity v (in cm s^{-1});

$\sigma(E)$ is the (n,γ) cross section (in cm^2) at neutron energy E (in eV);

$\Phi'(v)$ is the neutron flux per unit of velocity interval (in cm^{-3}) at neutron velocity v;

n'(v) is the neutron density per unit of velocity interval (in cm^{-4} s) at neutron velocity v;

$\Phi'(E)$ is the neutron flux per unit of energy interval (in cm^{-2} s^{-1} eV^{-1}) at neutron energy E.

In Eq. (2.24), $\sigma(v) = \sigma(E)$ with E (in erg $= 6.2415.10^{11}$ eV) $= \frac{1}{2}\ m_n\ v^2$ [m_n rest mass of the neutron $= 1.6749\ 10^{-24}$ g]. Furthermore, per definition, φ'(v) dv $=$ φ'(E)dE (both in cm^{-2} s^{-1}).

In Eq. (2.24), the functions σ(v) [$=$ σ(E)] and φ'(v) [φ'(E)] are complex and are respectively depending on the (n,γ) reaction and on the irradiation site.

Production of radioactive nuclei is described by,

$$\frac{dN}{dt} = R \cdot N_0 - \lambda \cdot N \qquad (2.25)$$

The disintegration rate of produced radionuclide at the end of irradiation is given by

$$A(t_{ir}) = N(t_{ir}) \cdot \ \lambda \cdot \ = N_0 \cdot \ R \cdot \ (1 - e^{-\lambda \cdot t_{ir}}) \qquad (2.26)$$

The dependence of activation cross-section and neutron flux density on the neutron energy can be taken into account in equation (2.24) by dividing the neutron spectrum into thermal and epithermal parts. The division is made at energy $E_{Cd} = 0.55$ eV (called Cd cut-off energy). This approach is commonly known as Høgdal´s convention. So integral in equation (2.24) can be rewritten as

$$R = \int_0^{V_{Cd}} n(v) \cdot v \cdot \sigma(v)dv + \int_{V_{Cd}}^0 n(v) \cdot v \cdot \sigma(v)dv \qquad (2.27)$$

The first term can be integrated directly

$$\int_0^{V_{Cd}} n(v) \cdot v \cdot \sigma(v)dv = v_0 \cdot \sigma_0 \cdot \int_0^\infty n(v)dv = v_0 \cdot \sigma_0 \cdot n \qquad (2.28)$$

where,

$$n = \int_0^\infty n(v)dv \qquad (2.29)$$

is called the thermal neutron density, with $\Phi_{th} = nv_0$,

- Φ_{th} is the conventional thermal neutron fluence rate, $m^{-2}\ s^{-1}$, for energies up to the Cd cutoff energy of 0.55 eV;

- σ_0 is the thermal neutron activation cross section, m^2, at 0.025 eV;

- v_0 is the most probable neutron velocity at 20 °C: 2200 m s^{-1}.

The second term is re-formulated in terms of neutron energy rather than neutron velocity and the infinite dilution resonance integral I_0 – which effectively is also a cross section (m^2) – is introduced:

$$\int_{v_{Cd}}^\infty n(v)vdv = \varphi_{epi} \int_{E_{Cd}}^{E_{max}} \frac{\sigma(E_n)dE_n}{E_n} \qquad (2.30)$$

with,

$$I_0 = \int_{E_{Cd}}^{E_{max}} \frac{\sigma(E_n)dE_n}{E_n} \qquad (2.31)$$

It is clear from this definition that the energy dependence of epithermal neutron flux density is proportional to $1/E$.

In the practice of nuclear reactors, the density of the epithermal neutron flux is not following the inverse proportionality exactly. A small deviation can be measured and therefore a parameter α is introduced as,

$$I_0(\alpha) = (1eV)^\alpha \int_{E_{Cd}}^{E_{max}} \frac{\sigma(E_n)dE_n}{E_n^{(1+\alpha)}} \qquad (2.32)$$

The term for reaction rate can be rewritten as,

$$R = \varphi_{th}\sigma_0 + \varphi_{epi}I_0(\alpha) \tag{2.33}$$

Expressing the ratio of the thermal neutron fluence rate and the epithermal neutron fluence rate as f=Φ_{th}/Φ_{epi} and the ratio of the resonance integral and the thermal activation cross section as $Q_0(\alpha)$= $I_0(\alpha)$/σ_0, an effective cross section can be defined:

$$\sigma_{eff} = \sigma_0(1 + \frac{Q_0(\alpha)}{f}) \tag{2.34}$$

t simplifies the Eq. **(2.33)** for the reaction rate to:

$$R = \varphi_{th}\sigma_{eff} \tag{2.35}$$

The nuclear transformations are established by measurement of the number of nuclear decays. The number of activated nuclei $N(t_i,t_d)$ present at the start of the measurement is given by:

$$N(t_i,t_d,t_m) = \frac{RN_0}{\lambda}(1 - e^{-\lambda t_i})e^{-\lambda t_d} \tag{2.36}$$

and the number of nuclei ΔN disintegrating during the measurement is given by:

$$\Delta N(t_i,t_d,t_m) = \frac{RN_0}{\lambda}(1 - e^{-\lambda t_i})e^{-\lambda t_d}(1 - e^{-\lambda t_m}) \tag{2.37}$$

in which td is the decay or waiting time, i.e. the time between the end of the irradiation and the start of the measurement tm is the duration of the measurement. Replacing the number of target nuclei N_0 by $(N_{Av}m)$/M and using the Eq. **(2.35)** for the reaction rate, the resulting net counts C in a peak in the spectrum corresponding with a given photon energy is approximated by the activation formula:

$$N_p = \Delta N\gamma\varepsilon = \varphi_{th}\sigma_{eff}\frac{N_{av}\theta m_x}{M_a}(1 - e^{-\lambda t_i})e^{-\lambda t_d}(1 - e^{-\lambda t_m})I\varepsilon \tag{2.38}$$

with:

• N_p is the net counts in the γ-ray peak of Eγ ;

• N_{Av} is the Avogadro's number in mol^{-1};

• θ is isotopic abundance of the target isotope;

16

• m_x is the mass of the irradiated element in g;

• M_a is the atomic mass in g mol^{-1};

• I is the gamma-ray abundance, i.e. the probability of the disintegrating nucleus emitting a photon of E_γ (photons disintegration^{-1});

• ε is the full energy photopeak efficiency of the detector, i.e. the probability that an emitted photon of given energy will be detected and contribute to the photopeak at energy E_γ in the spectrum.

Although the photons emitted have energies ranging from tens of keVs to MeVs and have high penetrating powers, they still can be absorbed or scattered in the sample itself depending on the sample size, composition and photon energy. This effect is called gamma-ray self attenuation.

Also, two or more photons may be detected simultaneously within the time resolution of the detector; this effect is called summation. Eq. **(2.38)** can be simply rewritten towards the measurement equation of NAA, which shows how the mass of an element measured can be derived from the net peak area C:

$$m_x = N_p \cdot \frac{M_a}{N_{av\cdot\theta}} \cdot \frac{\lambda}{\varphi_{th}\sigma_{eff}I\cdot\varepsilon(1-e^{-\lambda t_i})e^{-\lambda t_d}(1-e^{-\lambda t_m})} \qquad \textbf{(2.39)}$$

2.4.1 Standardization

Standardization is based on the determination of the proportionality factors F that relate the net peak areas in the gamma-ray spectrum to the amounts of the elements present in the sample under given experimental conditions:

$$F=N_p/M \qquad \textbf{(2.40)}$$

Both absolute and relative methods of calibration exist.

2.4.1.1 Direct comparator method

The unknown sample is irradiated together with a standard material (calibrator) that contains a known amount of the element(s) of interest. Both are measured under the same conditions (sample-to-detector distance, equivalent sample size and if possible

equivalent in composition). From the comparison of the net peak areas in the two measured spectra the mass of the element of interest can be calculated:

$$m_{x(unk)} = m_{x(cal)} \cdot \frac{(\frac{N_p}{t_m e^{-\lambda t_d}(1-e^{-\lambda t_m})})_{unk}}{(\frac{N_p}{t_m e^{-\lambda t_d}(1-e^{-\lambda t_m})})_{cal}}$$ (2.41)

in which m_x(unk), m_x(cal) mass of the element of interest, in the unknown sample and the standard material, respectively in g.

In this procedure, when calculating the mass, neutron fluence rate, cross section, and photopeak efficiency cancel out, and the remaining parameters are all known. This calibration procedure is used when the highest degree of accuracy is desired.

For laboratories intended to get the full multi-element powers of INAA, the relative calibration on the basis of element calibrators is not directly suitable. It takes considerable effort to prepare multi-element calibrators for all 70 elements measurable via NAA with an adequate degree of accuracy in a volume closely matching the size and the shape of the samples.

2.4.1.2 Single comparator method

Multi-element INAA on basis of the relative calibration method is feasible when performed according to the principles of the single comparator method. Assuming stability in time of all relevant experimental conditions, calibrators for all elements are co-irradiated each in turn with the chosen single comparator element. Once the sensitivity for all elements relative to the comparator element has been determined (expressed as the so-called k-factor, see below), only the comparator element has to be used in routine measurements instead of individual calibrators for each element. The single comparator method for multi-element INAA was based on the ratio of proportionality factors of the element of interest and of the comparator element after correction for saturation, decay, counting and sample weights defined the k-factor for each element i as:

$$k_i = \frac{(M_a)_{i,cal}\gamma_{comp}\theta_{comp}\sigma_{eff,comp}}{M_{i,cal}\gamma_{i,cal}\varepsilon_{i,cal}\theta_{i,cal}(\sigma_{eff})_{i,cal}}$$ (2.42)

Masses for each element i then can be calculated from these ki factors; for an element determined via a directly produced radionuclide the mass m_x(unk) follows from:

$$m_{x(unk)} = m_{x(comp)} \cdot \frac{(\frac{N_p}{(1-e^{-\lambda tm})t_m e^{-\lambda t_d}(1-e^{-\lambda tm})})_{unk}}{(\frac{N_p}{(1-e^{-\lambda tm})t_m e^{-\lambda t_d}(1-e^{-\lambda tm})})_{cal}} \cdot k_i \qquad \textbf{(2.43)}$$

where: m_x(comp) is the mass of element x, in comparator in g.

These experimentally determined k-factors are often more accurate than when calculated on basis of literature data as in the absolute calibration method.

However, the k-factors are only valid for a specific detector, a specific counting geometry and irradiation facility, and remain valid only as long as the neutron fluence rate parameters of the irradiation facility remain stable. The single comparator method requires laborious calibrations in advance, and finally yield relatively (compared to the direct comparator method) higher uncertainties of the measured values. Moreover, it requires experimental determination of the photopeak efficiencies of the detector. Metrological traceability of the measured values to the S.I. may be demonstrated.

2.4.1.3 The k₀-comparator method

The k_0-based neutron activation analysis (k_0-NAA) technique, developed in 1970s, is being increasingly used for multielement analysis in a variety of matrices using reactor neutrons. In the method, the evaluation of the analytical result is based on the so-called k_0- factors that are associated with each gamma line in the gamma spectrum of the activated sample. These factors replace nuclear constants, such as cross sections and gamma emission probabilities and are determined in specialized NAA laboratories. This technique has been reported to be flexible with respect to changes in irradiation and measuring conditions. It is simpler than the relative comparator method in terms of experiments but involves more complicated formulae and calculations. [9].

The k_0-NAA technique, in general, uses input parameters such as (1) the epithermal neutron flux shape factor (α), (2) sub-cadmium-to-epithermal neutron flux ratio (f), (3) modified spectral index r(α) $\sqrt{}$ (T_n / T_0), (4) Westcott's g(T_n)-factor, (5) the full

energy peak detection efficiency (ε_p), and (6) nuclear data on Q_0 (ratio of resonance integral (I_0) to thermal neutron cross section (σ_0) and k_0. The parameters from (1) to (4) are dependent on each irradiation facility and the parameter (5) is dependent on each counting facility. The neutron field in a nuclear reactor contains an epithermal component that contributes to the sample neutron activation. Furthermore, for nuclides with the Westcott's $g(T_n)$-factor different from unity, the Høgdahl convention should not be applied and the neutron temperature should be introduced for application of a more sophisticated formalism, the Westcott formalism.

These two formalisms should be taken into account in order to preserve the accuracy of k_0-method. The k_0-NAA method is at present capable of tackling a large variety of analytical problems when it comes to the multi-element determination in many practical samples.

During the three last decades Frans de Corte and his co-workers focused their investigations to develop a method based on co-irradiation of a sample and a neutron flux monitor, such as gold and the use of a composite nuclear constant called k_0-factor. In addition, this method allows to analyze the sample without use the reference standard like INAA method [9].

The k-factors have been defined as independent of neutron fluence rate parameters as well as of spectrometer characteristics. In this approach, the irradiation parameter $(1+Q_0(\alpha)/f)$ (Eq.(**2.34**)) and the detection efficiency ε are separated in the expression (**2.42**) of the k-factor, which resulted at the definition of the k_0-factor.

$$k_0 = \frac{1}{k} \cdot \frac{1+Q_{0,comp}(\alpha)/f}{1+Q_{0,cal}(\alpha)/f} \cdot \frac{\varepsilon_{comp}}{\varepsilon_{comp}} = \frac{M_{comp}}{\theta_{comp}\sigma_{0,comp}\gamma_{comp}} \cdot \frac{\theta_{cal}\sigma_{0,cal}\gamma_{cal}}{M_{cal}} \qquad \textbf{(2.44)}$$

$$m_{x(unk)} = m_{x(comp)} \frac{1+Q_{0,comp}(\alpha)/f}{1+Q_{0,cal}(\alpha)/f} \cdot \frac{\varepsilon_{comp}}{\varepsilon_{comp}} \cdot \frac{\left(\frac{N_p/t_m}{(1-e^{-\lambda t_i})e^{-\lambda t_d}(1-e^{-\lambda t_m})m}\right)_{unk}}{\left(\frac{N_p}{(1-e^{-\lambda t_i})e^{-\lambda t_d}(1-e^{-\lambda t_m})m}\right)_{comp}} \cdot \frac{1}{k_0} \quad \textbf{(2.45)}$$

The applicability of HØGDAHL convention is restricted to (n,γ) reactions for which WESTCOTT's g-factor is equal to unity (independent of neutron temperature), the

cases for which WESTCOTT's g = 1, such as the reactions ^{151}Eu(n, γ) and ^{176}Lu(n, γ) are excluded from being dealt with. Compared with relative method k_0-NAA is experimentally simpler (it eliminates the need for multi-element standards, but requires more complicated calculations.

Summarizing, relative calibration by the direct comparator method renders the lowest uncertainties of the measured values whereas metrological traceability of these values to the S.I. can easily be demonstrated. As such, this approach is often preferred from a metrological viewpoint.

The concentration of an element can be determined as:

$$p_x(ppm) = \frac{[\frac{N_p/t_m}{SDCW}]_X}{[\frac{N_p/t_m}{SDCW}]_{Au}} \cdot \frac{1}{k_{0,Au(x)}} \cdot \frac{G_{th,Au}f + G_{epi,Au}Q_{0,Au}(\alpha)}{G_{th,x}f + G_{epi,x}Q_{0,x}(\alpha)} \cdot \frac{\varepsilon_{p,Au}}{\varepsilon_{p,x}} \times 10^6 \qquad (2.46)$$

Where: the indices x and Au refer to the sample and the monitor, respectively; W_{Au} and W_x represent the mass of the gold monitor and the sample (in g); N_p is the measured peak area, corrected for dead time and true coincidence; S, D, C are the saturation, decay and counting factors, respectively; t_m is the measuring time; G_{th} and G_e are the correction factors for thermal and epithermal neutron self shielding, respectively.

2.4.2 NAA in Archaeology

As an archaeological tool, J. Robert Oppenheimer suggested NAA's use to R. W. Dodson and E. V. Sayre of Brookhaven National Laboratory in 1954, right after the dawn of the nuclear age. Sayre was the one doing the experimental work, using terracotta ceramics recovered from archaeological contexts in the Mediterranean and the Near East. The investigators established that decay patterns of irradiated sherds were distinct in accordance with their geographical origin. They reported the results at a meeting of archaeologists and chemists at the Institute for Advanced Study at Princeton in 1956. Around the same time, a group at Oxford started employing neutron activation analysis in provenance investigations of pottery and coins. Early attempts to use the technique for archaeological purposes were hampered by the poor resolution of available detection systems. The advent of the lithium-drifted

germanium (Ge-Li) detector in the 1960s prompted a flurry of archaeological applications. It provided a definitive description of standard comparator instrumental neutron activation analysis (INAA) as applied to archaeological provenance determination at the Lawrence Berkeley Laboratory (LBL). Techniques similar to those described by Perlman and Asaro were used at Brookhaven National Laboratory (BNL) beginning in the late 1960s.

During the 1970s and 1980s, archaeologists turned more and more frequently to INAA to help determine the sources of pottery, Obsidian, chert, and other materials. By the early 1990s, INAA was regarded as the technique of choice for such applications. "Methodology" concerns the means by which the analytical measurements produced by INAA can be used to determine the sources of archaeological artefacts [10].

The method has been much revised since these early experiments, and improvements in accuracy now provide the opportunity to address ever-more precise spatial relationships, making INAA a staple of archaeochemistry. In some cases, INAA laboratories have developed their archaeological specialities. These data have been used to reconstruct village trading patterns and migratory routes, as aids in chronology building, and to infer how ancient societies organised the production of particular goods. Volcanic materials, such as obsidians and pumices, have elemental compositions specific to their geological sources. Large eruptions also leave a physical, stratigraphically visible signature of tephra (volcanic ash) in the archaeological record [11].

INAA can link these visible geological layers to particular, historically documented eruptions, thus aiding in the creation of specific chronological markers for fieldworkers. Establishing the transport of pumices, obsidians, and basalts away from their source is a principle means for the reconstruction of long-distance trading networks and distribution economies. The elemental signature from INAA analysis of clays and ceramic paints allows for the identification of pottery production centres and distribution patterns. Finely made pottery often served as a status good in many parts of the ancient world, and as such reconstructing the movement of fine wares provides a proxy for the circulation of the people that transported them. As such, recent applications of INAA have been instrumental in identifying phenomena such as pilgrimages.

Specific organic molecules associated with archaeological contexts or artefacts have been identified primarily through the use of mass spectrometric methods. Thus, questions can be addressed by the production, distribution, and use of organic substances in the ancient world.

2.4.3 NAA in Marine Biota

The trace element accumulation in biological samples may provide insight into the relationship between certain species and their surroundings. Patterns of elemental uptake are often reflected in the elemental composition of incrementally grown biological structures. Biological structures of this type contain discernible physical attributes that are deposited with a seasonal or more frequent periodicity. Elemental analytical data are having spatial correspondence to these features, and the time line implicit within may be amenable to meaningful interpretation [12].

Data of this dimension can provide indirect evidence of climatological variation, or reveal extraordinary temporal changes in elemental uptake possibly related to anthropogenic perturbation of the environment.

With the rising concern in industrial nations of the impact of man on his environment and its biological effect on him, it increased the realisation of the importance of trace element chemistry in biological systems. Of primary significance is the role played by trace elements and whether or not they are beneficial to the biochemistry of man. A number of trace elements are required nutrients. To date, the essential trace elements for plant and animal life include Co, Cr, Cu, B, F, Fe, I, Mn, Mo, Se, and Zn, with Ni, Sn, and V, possibly essential. The minor elements Na, K, Mg, Ca, P, S, and C1 are also of interest in life systems. To this list of essential elements must be added those of toxicological concern, i.e., Li, Be, Ba, Ni, Ag, Cd, Hg, As, Sb, Bi, Pb, and Br. It is entirely possible that additional trace elements may be found to exercise essentiality or toxicity as further research is performed on their biological role. To expedite the study of these trace elements, comprehensive multi-element analytical methods of high sensitivity in complex biological matrices are necessary [13].

3.   MATERIAL AND METHOD

3.1   Site Information

Throughout the history, Istanbul has served as the Capital of the Roman Empire (330–395), the East Roman (Byzantine) Empire (395–1204 and 1261–1453), the Latin Empire (1204–1261), and the Ottoman Empire (1453–1922) [14]. Due to its strategic location at the crossroads connecting Anatolia with Southeastern Europe and the Black Sea basin to the Mediterranean, it has always been of prime importance in the history of civilization. Along with its historicity, the geographical setting of the city is of significance, featuring unique but at the same time environmentally critical characteristics. It is located at the narrow neck of a shallow and long water channel, the Bosphorus, connecting two inland seas, Marmara, and the Black Sea.

With the lowering of the global sea level during the late glacial period, the Sea of Marmara (SOM) was transformed into a brackish lake. While the shelf areas of the SOM were terrestrial environments. These conditions formed a marine environment as a result of rising sea level at ~14 cal ka BP, from the Canakkale (Dardanelles) Strait. Sea level reached present-day conditions at about ~seven cal ka BP with the drowning of various coastal depositional environments based on the faunal composition of littoral sediments from boreholes drilled in the coastal areas of the SOM. To understand the previous conditions, it is important to study on the Marmara basin and especially in Istanbul. The city has a strategic location between Anatolia–Near East and southeastern Europe [15].

During the preliminary construction works of the Marmaray Tube Tunnel Project (Figure 3.1, the remnants of the ancient Theodosian Harbor) were exposed at Yenikapı by the İstanbul Archaeology Museum (IAM).

Figure 3.1 : Marmaray Project Plan and Profile [16].

This large-scale project has built a tube tunnel under the sea between the Asian and European parts of the city. IAM has commenced a rescue excavation after the discovery of the remnants of the Byzantine harbor [16] (See Figure 3.2).

Figure 3.2 : Archaeological Site at Yenikapı [16].

Based on historical sources, construction of this port is assigned to either the time of Emperor Constantine I (AD 306–307) or Theodosius I (AD 379–395). The sedimentary found at the site has revealed tangible evidence for changes in sea level and environmental conditions in the SOM over the years. At yet deeper levels, a unique collection of archeological material that belong to the Neolithic Period has also been discovered. Numerous researchers from different disciplines have investigated Ancient harbors of the Mediterranean Sea and have found valuable information on coastal stratigraphy, paleogeography, sea-level changes and effects of local tectonics [17]. The study site has both geological and archeological evidences for changes in the sea level and possible effects on marine life.

3.2 Study Area

The Yenikapı excavation site is located on the southern coast of the historic center of İstanbul within the so-called "old town of İstanbul". It is a peninsula (Sarayburnu) bounded to the north by the Golden Horn and to the south by the SOM. A small stream, called Bayrampaşa Deresi—ancient Lykos, had been draining into the SOM through the old "historical peninsula—Sarayburnu" area until the bed of the stream was filled in to build a road in 1950s. Its valley has a length of 5.6 km and a maximum width of 1.5 km (Figure 3.3). The excavation site corresponds to the right side of Lykos valley. It was divided into squares by archeologists for study related purposes as given in (Figure 3.4).

Location of Theodosius' harbour; hypothetical coastline during the Byzantine period and the Istanbul city walls. Wind rose from windfinder.com

Istanbul Theodosius' city walls

Istanbul Constantine's city walls

Hypothetical coastline during the Byzantine period

Lycos river
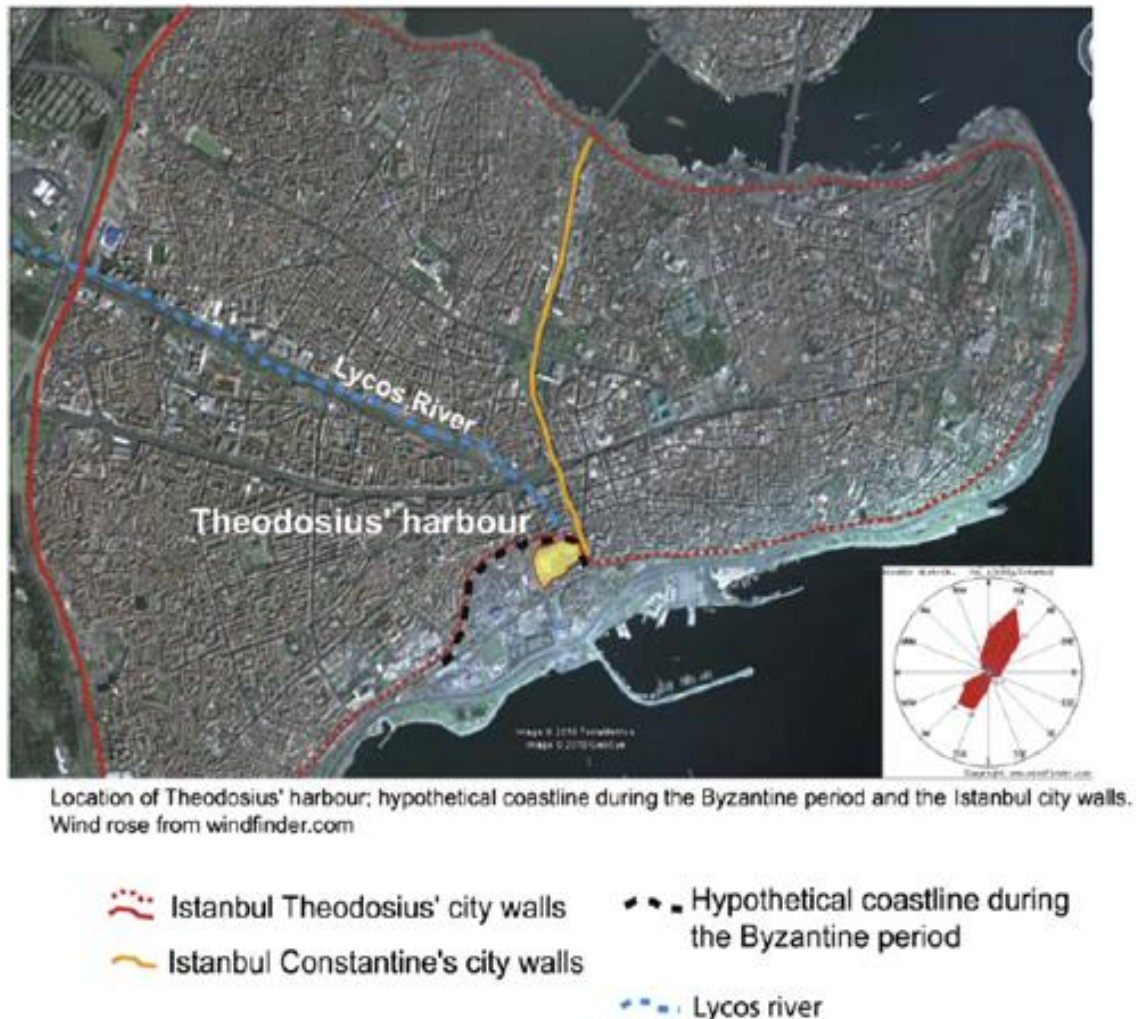
Figure 3.3 : Location of Theodosius [17].

27
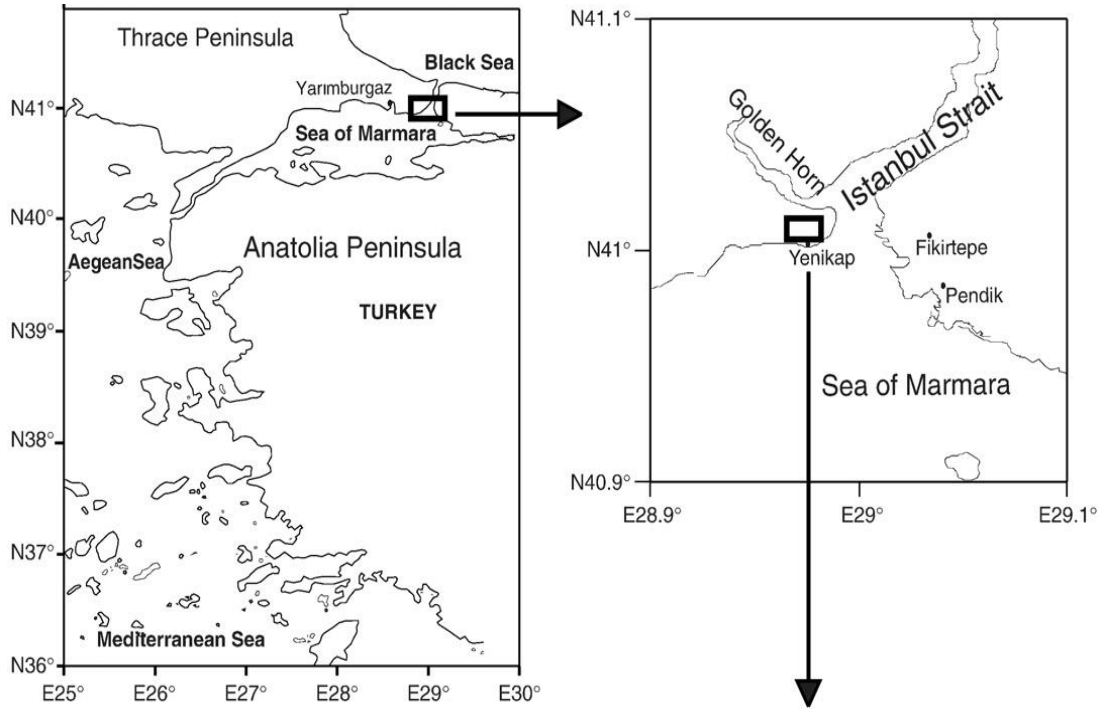
Figure 3.4 : The location of the excavation site in İstanbul. Digital image is produced from Google Earth 4.3 [18].

The excavation site was divided into squares by archaelogisists for study related purposes as given in Figure 3.5.

28
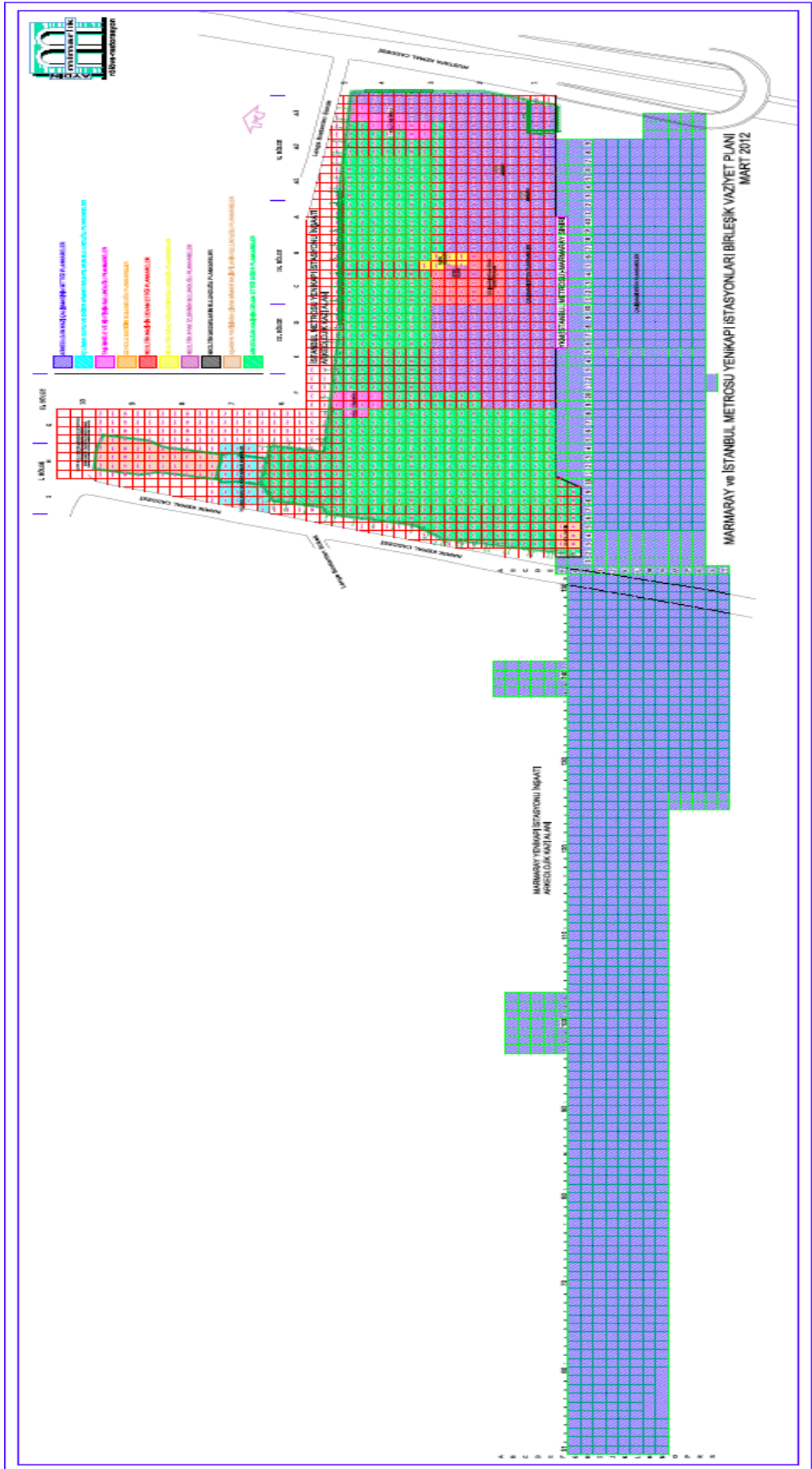
Figure 3.5 : Excavation Site Map (Courtesy of Istanbul Archaeological Museum).

3.3 Sample Properties

For this project, we selected 24 samples consist of shells, clams, mussels, limpets, coral, sea molluscs, fish vertebras and tortoise shells, from different layers and areas of Marmaray-Yenikapi excavation site. Figure 3.6 shows exact locations of samples at site. Every sample was given a letter between A and U, for identification (Figure 3.7, Figure 3.8, Figure 3.9, Figure 3.10, Figure 3.11). List of samples with the given names and depth can be shown as given in Table 3.1.
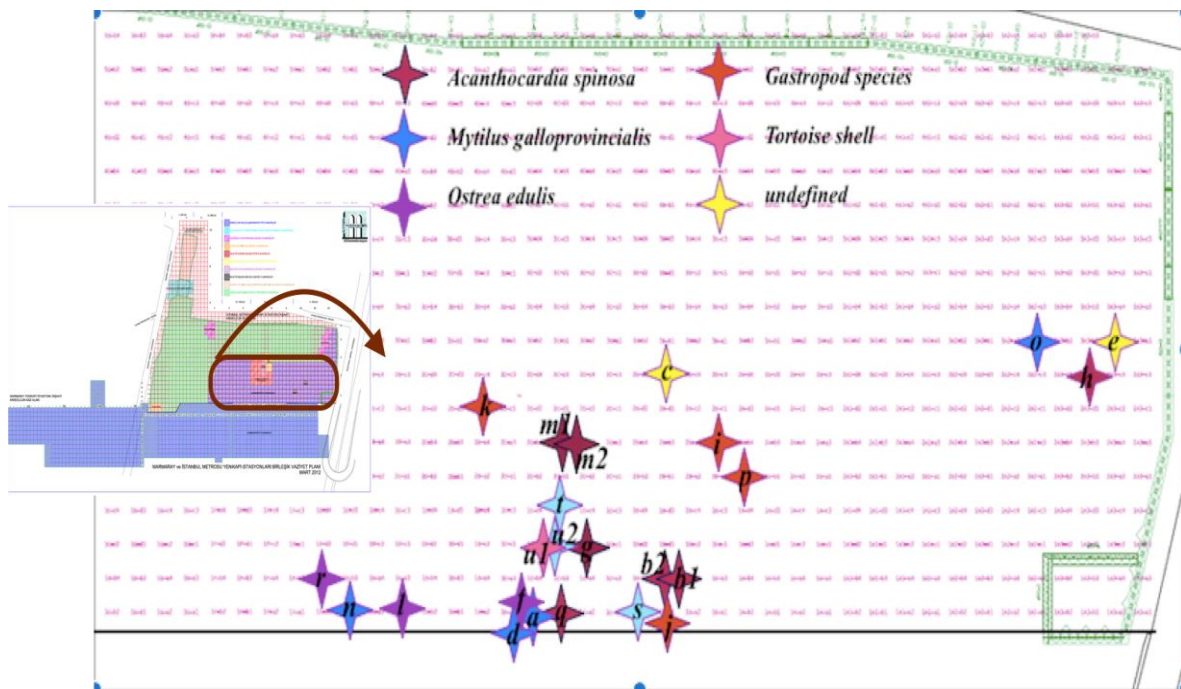
Figure 3.6 : Location of collected findings.

Figure 3.7 : Samples from left to right respectively, 10C, 10F, 10L, 10R, 10E.

Figure 3.8 : Samples from left to right respectively, 10K, 10P, 10I, 10Q, 10J.

Figure 3.9 : Samples from left to right respectively, 10Q, 10N, 10A, 10D.

Figure 3.10 : Samples from left to right respectively, 10H, 10M(1)(below), 10M(2)(above), 10B(1)(left), 10B(2)(right), 10G(right).

Figure 3.11 : Samples from left to right respectively, 10U(1)(tortoise shell), 10U(2)(fish vertebra), 10T(fish vertebra), 10S(fish vertebra).

Table 3.1 : List of named samples according to soil depth.
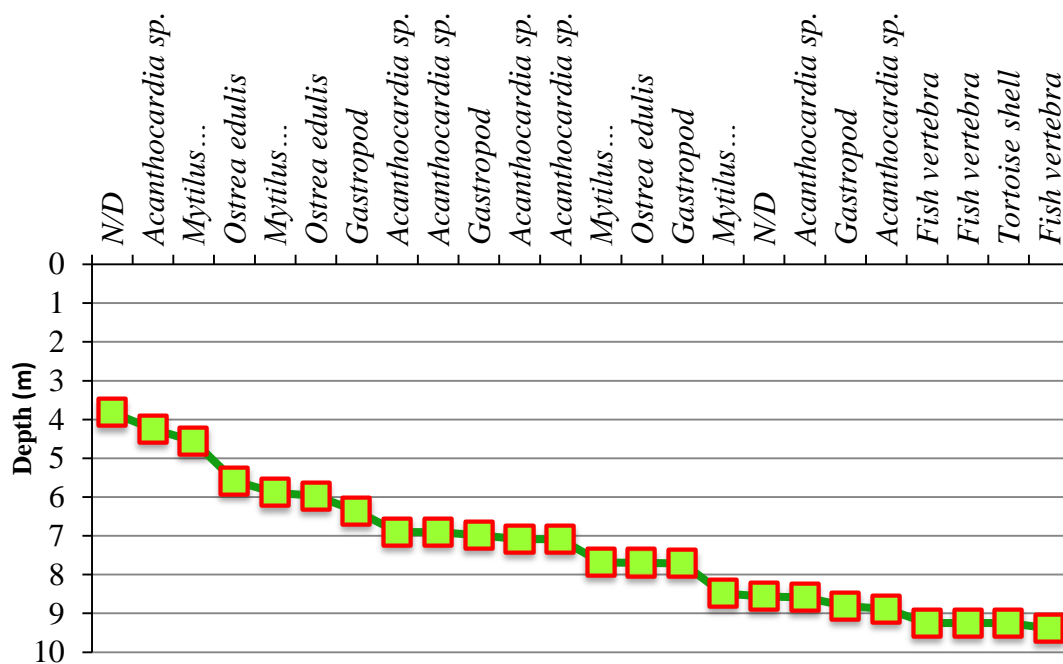
3.4 Preparation of Samples

Samples were prepared conventionally including a through cleaning procedure in distilled water and an ultrasonic bath, see in Figure 3.12. Some of the cleaned samples can be found in Figure 3.13.

Figure 3.12 : Ultrasonic bath.

Figure 3.13 : Some of the samples after cleaning process, left to be dried.

For most of the samples we just selected the small chips produced after the break for the thin section and ground them in an agate mortar to obtain a fine and homogeneous powder. This procedure takes only few minutes, but then they need to be cleaned carefully both the mortar and the pestle in order to avoid any contamination between the samples. Some of the hard shells were sampled by drilling. The obtained powder is temporarily collected in small plastic containers (See in Figure 3.14).

After one night in the oven at 90 °C, the sample is weighted by means of a precision balance (about 100 mg of powder was needed) and transferred into SuprasilTM quartz glass vials.

Figure 3.14 : Agate mortar. Plastic container and drilling

Before going into the reactor and to be irradiated, all the vials must be sealed. The sealing is made by fire, using a soldering iron arrangement in the same laboratory in which the samples were prepared. Once finished, we used an engraving tool to write the number of the sample on the side of each vial. Figure 3.15 shows both procedure. At this point everything is ready to start with the irradiation, just the time for the samples to 'rest' a little bit immersed into a pure water solution.
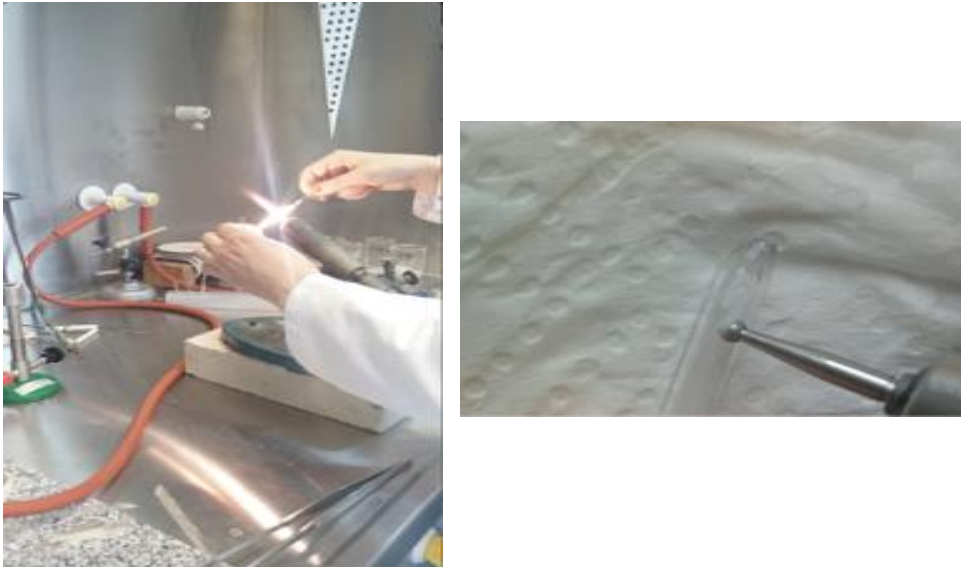
Figure 3.15 : Sealing and engraving sample numbers to SuprasilTM quartz glass vials, before irradiation.

3.5   Irradiation and Counting

Although INAA is the only analytical tool that can provide reliable data in absolute measurements, certified reference materials are used as standard materials in comparator method [19]. After sample preparation, the samples are irradiated for 30–40 h in the central irradiation tube (located in the center of the core) of the TRIGA Mark II reactor of the Atominstitut (Vienna University of Technology, Wien, Austria) at a thermal neutron flux of $1 \cdot 10^{13}$ cm$^2 \cdot$s^{-1} together with a set of reference materials Figure 3.16 shows the TRIGA Mark II reactor of the Atominstitut.

Figure 3.16 : TRIGA Mark II reactor of the Atominstitut [20].

The amounts of elements in certified reference materials (Cl-Chondrit, Kruste85, KrusteOben, KrusteGesamt, Bo-Norm, Shale, and BMSP) were given in Table 3.2, Table 3.3 and Table 3.4 [21,22,23,24,25].

Table 3.2 : Essential element concentrations in used Standard Reference Materials (mg·kg^{-1}).

	Na	K	Cr	Fe	Co	Ni	Zn
Cl-Chondrit	5100	550	2650	181000	500	-	310
Kruste85	28300	25900	100	50000	25.00	-	70.00
KrusteOben	28900	28000	35	35000	10.00	-	71.00
KrusteGesamt	23000	9100	185	70700	29.00	-	80.00
Bo-Norm	33281	24287	1.973	21839	3.933	-	69.41
Shale	7803	31546	125	39565	25.70	1.00	1.00
BMSP	1010	21700	145	43400	9.37	-	NA

Table 3.3 : Non-essential element concentrations in used Standard Reference Materials (mg·kg^{-1}).

	Sc	As	Rb	Sr	Zr	Sb	Cs	Ba	Hf	Ta
Cl-Chondrit	5.92	1.850	2.300	-	3.820	0.140	0.190	2.410	0.103	0.014
Kruste85	22.00	1.800	90.00	-	165.0	0.20	3.00	425	3.000	2.000
KrusteOben	11.00	1.500	112.00	-	190.0	0.20	3.70	550	5.800	2.200
KrusteGesamt	30.00	1.000	32.00	-	100.0	0.20	1.00	250	3.000	1.000
Bo-Norm	8.58	2.773	108.23	-	289.7	0.30	2.89	564	7.747	0.804
Shale	14.90	28.40	125.00	300	200.0	2.09	5.16	636	6.300	1.120
BMSP	18.70	12.00	161.00	-	NA	1.65	35.40	580	4.540	1.710

Table 3.4 : Lanthanide and actinide element concentrations in used Standard Reference Materials (mg·kg^{-1}).

	La	Ce	Nd	Sm	Eu	Tb	Yb	Lu	Th	U
Cl-Chondrit	0.237	0.613	0.457	0.148	0.056	0.036	0.161	0.025	0.029	0.007
Kruste85	30.000	60.000	28.000	6.000	1.200	0.900	3.400	0.500	7.200	1.800
KrusteOben	30.000	64.000	26.000	4.500	0.880	0.640	2.200	0.320	10.700	2.800
KrusteGesamt	16.000	33.000	16.000	3.500	1.100	0.600	2.200	0.300	3.500	0.910
Bo-Norm	31.71	62.96	25.65	6.18	1.003	1.013	5.059	0.830	19.97	5.909
Shale	31.10	66.70	27.40	5.59	1.180	0.850	3.060	0.456	12.30	2.660
BMSP	50.50	106.20	NA	8.92	1.720	1.400	4.520	0.729	17.70	3.780

After irradiation, the quartz glass sample vials were decontaminated and packed into polyethylene (PE) vials fitting the automatic sample changer device of the Atominstitute. After a cooling time of 5 days, a first gamma spectrum was measured to obtain the activities of the short and medium-lived activation products ^{153}Sm, ^{239}Np (U), ^{76}As, ^{24}Na, ^{42}K, and ^{140}La. Figure 3.18 shows the gamma spectrometry system.

Figure 3.17 : Gamma spectrometry system for NAA [26].

Qualitative and quantitative results were obtained after proper energy and efficiency calibrations of the counting systems. Three weeks later, a second measurement sequence was started to detect the long-lived activation products ^{141}Ce, ^{169}Yb, ^{177}Lu, ^{233}Pa (Th), ^{51}Cr, ^{181}Hf, ^{131}Ba, ^{147}Nd, ^{95}Zr, ^{134}Cs, ^{160}Tb, ^{86}Rb, ^{59}Fe, ^{65}Zn, ^{46}Sc, ^{60}Co, ^{182}Ta, ^{152}Eu, and ^{124}Sb. The measuring times were 1800 s and 10.000 s, respectively [27]. All samples were measured in a fixed position at a distance of 4 cm beside the detector.
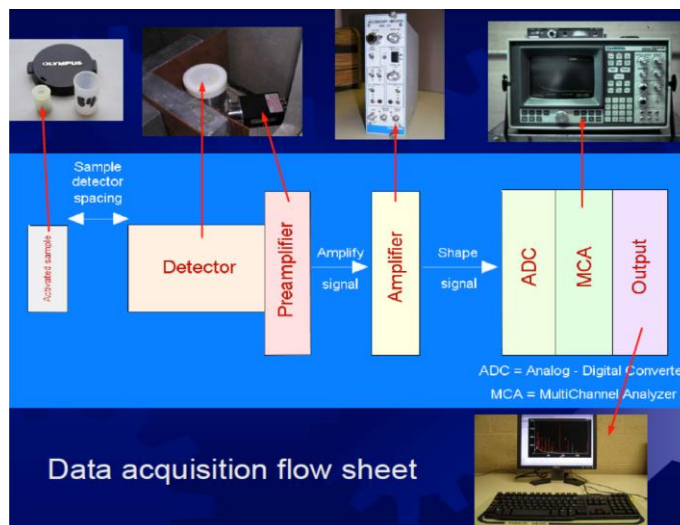
Figure 3.18 : Data acquisition flow sheet [26].

The gamma-spectrometry was performed with a 151 cm³ HPGe-detector (1.8 keV resolution at the 1332 keV ^{60}Co peak; 50.1% relative efficiency), connected to a PC based multi-channel analyser with a preloaded filter and a Loss-Free Counting system. These analyses must be performed by means of short time activation analysis, due to the short half-life of the respective activation products (see Table 3.5). Blank values of the quartz glass vials were measured and found negligible to consider in calculations.

Table 3.5 Elements, activation products, half-lives, and γ-photon energies (sorted by measurement sequences) [28].

Element	Activation product	Half-life ($T_{1/2}$)	γ-Energy (keV)
(i) *Short time activation analysis(if required)*			
Al	^{28}Al	2.31 min	1778.8
Ca	^{49}Ca	8.72 min	3084.4
Dy	^{165}Dy	2.33 h	94.7
Mn	^{56}Mn	2.58 h	1811.2
Ti	^{51}Ti	5.79 min	320
V	^{52}V	3.75 min	1434.2
(ii) *Measurement 5 days after neutron irradiation*			
As	^{76}As	25.87 h	559.1
K	^{42}K	12.36 h	1524.7
La	^{140}La	40.26 h	1596.2
Lu	^{177}Lu	6.65 d	208.4
Na	^{24}Na	14.96 h	1368.6; 2754.1
Sm	^{153}Sm	46.28 h	103.2
U	^{239}Np	56.55 h	277.6

Table 3.5 (continued) Elements, activation products, half-lives, and γ-photon energies (sorted by measurement sequences) [28].

Element	Activation product	Half-life ($T_{1/2}$)	γ-Energy (keV)
(iv) Measurement 28 days after neutron irradiation			
Ba	^{131}Ba	11.5 d	496.3
Ce	^{141}Ce	32.5 d	145.5
Co	^{60}Co	5.27 a	1173.2
Cr	^{51}Cr	27.7 d	320.1
Cs	^{134}Cs	2.07 a	795.8
Eu	^{152}Eu	13.52 a	1408.1
Fe	^{59}Fe	44.5 d	1099.2
Hf	^{181}Hf	42.39 d	482.2
Lu	^{177}Lu	6.65 d	208.4
Nd	^{147}Nd	10.98 d	531
Rb	^{86}Rb	18.64 d	1076.6
Sb	^{124}Sb	60.2 d	1691
Sc	^{46}Sc	83.79 d	1120.5
Ta	^{182}Ta	114.43d	1221.3; 1189.1
Tb	^{160}Tb	72.3 d	879.4
Th	^{233}Pa	26.96 d	311.9
Yb	^{169}Yb	32.02 d	177.2
Zn	^{65}Zn	244.06d	1115.5
Zr	^{95}Zr	64.03 d	756.7

In Table 3.5 ^{239}Np is the decay product of ^{239}U ($T_{1/2}$ = 23.5 min), which is the activation product of ^{238}U, and can be detected more sensitively. ^{233}Pa is the decay product of ^{233}Th ($T_{1/2}$ = 22.3 min), which is the activation product of ^{232}Th, and can be detected more sensitively.

4.   RESULTS AND DISCUSSION

The elements As, Ba, Ce, Cs, Co, Cr, Eu, Fe, Hf, K, La, Lu, Na, Nd, Ni, Rb, Sb, Sc, Sr, Sm, Ta, Tb, Th, U, W, Yb, Zr and Zn were determined in Neolithic Age animal findings and shown by three concentration groups as essential elements, lanthanides and actinides and non-essential elements.

4.1   Elemental analysis of *Acanthocardia spinosa*

Element concentrations of *Acanthocardia spinosa* given in Table 4.1 showed that the highest concentration value belongs to Sr, followed by Ni and Zn. K is almost non-existent among the species. The depth is decreasing from 8,8 m (10G) to 4,2 m (10H) (See Table 3.1) with it, Sr levels increasing from 0.93 to 10,79 mg·kg^{-1}. Thus it may be a correlation between depth and strontium levels.

Table 4.1 : Element concentrations of *Acanthocardia spinosa* (mg·kg^{-1}).

Code	Na	K	Cr	Fe	Co	Ni	Zn			
2014/10B(1)	0.345	0.000	0.000	0.001	0.009	0.000	0.000			
2014/10B(2)	0.023	0.012	0.008	0.006	0.010	0.000	0.000			
2014/10G	0.351	0.000	0.008	0.039	0.039	2.180	0.000			
2014/10H	0.314	0.000	0.009	0.009	0.229	7.630	0.000			
2014/10M(1)	0.326	0.000	0.470	0.095	0.093	5.354	7.227			
2104/10M(2)	0.330	0.032	0.012	0.005	0.044	0.000	0.000			
2014/10Q	0.382	0.000	0.012	0.006	0.084	1.987	0.000			
	Sc	**As**	**Rb**	**Sr**	**Zr**	**Sb**	**Cs**	**Ba**	**Hf**	**Ta**
2014/10B(1)	0.004	0.007	0.000	5.781	0.098	0.000	0.000	0.173	0.000	0.000
2014/10B(2)	0.006	0.008	0.000	1.630	0.000	0.000	0.000	0.167	0.000	0.000
2014/10G	0.011	0.043	0.000	0.938	0.000	0.007	0.004	0.100	0.003	0.000
2014/10H	0.010	0.021	0.000	10.793	0.155	0.017	0.000	0.308	0.000	0.000
2014/10M(1)	0.065	0.019	0.066	4.573	0.261	0.122	0.070	0.252	0.193	0.067
2104/10M(2)	0.003	0.173	0.000	4.175	0.082	0.000	0.000	0.153	0.000	0.000
2014/10Q	0.005	0.119	0.000	6.373	0.062	0.020	0.000	0.181	0.000	0.000
	La	**Ce**	**Nd**	**Sm**	**Eu**	**Tb**	**Yb**	**Lu**	**Th**	**U**
2014/10B(1)	0.286	0.244	0.239	0.240	0.159	0.107	0.069	0.082	0.012	1.176
2014/10B(2)	0.718	0.703	0.728	0.429	0.356	0.168	0.080	0.095	0.028	0.029
2014/10G	0.866	0.073	0.000	0.575	0.087	0.094	0.093	0.067	0.017	0.181
2014/10H	0.496	1.374	1.910	0.396	1.158	0.558	0.211	0.109	0.079	0.249
2014/10M(1)	0.891	0.257	0.226	0.676	0.261	0.240	0.259	0.107	0.218	1.481
2104/10M(2)	0.222	0.444	0.514	0.242	0.299	0.157	0.072	0.234	0.032	0.278
2014/10Q	0.215	0.237	0.143	0.186	0.132	0.092	0.053	0.048	0.011	0.878

4.2 Elemental analysis of fish vertebra

The concentrations of elements in fish vertebras (Table 4.2) show similar values with the other studies on the same subject [29]. Like lanthanides and actinides it seems Sc, Zr and Ba are increasing with depth also, with further analysis these results can be linked to the age of the species.

Table 4.2 : Element concentrations of fish vertebra (mg·kg^{-1}).

Code	Na	K	Cr	Fe	Co	Ni	Zn		
2014/10S	0.322	0.057	0.366	0.708	1.885	50.5	56.1		
2014/10T	0.356	0.000	0.100	0.260	0.148	18.8	72.7		
2014/10U(2)	0.450	0.000	0.414	0.326	0.168	23.0	66.0		
	Sc	As	Rb	Sr	Zr	Sb	Cs	Ba	Hf	Ta
2014/10S	0.322	1.424	0.131	1.927	2.731	0.289	0.255	2.061	0.251	0.170
2014/10T	0.332	0.929	0.036	2.682	4.004	0.160	0.079	2.368	0.093	0.050
2014/10U(2)	0.429	1.228	0.073	2.563	5.007	0.163	0.137	2.666	0.223	0.095
	La	Ce	Nd	Sm	Eu	Tb	Yb	Lu	Th
2014/10S	3.542	2.391	3.075	3.674	2.830	3.703	4.805	11.442	0.291
2014/10T	6.977	5.095	5.726	6.499	5.507	6.730	7.571	17.104	0.241
2014/10U(2)	7.791	5.508	6.303	7.819	6.196	7.570	8.629	20.846	0.357

4.3 Elemental analysis of Gastropods

Element concentrations of Gastropods (Table 4.3) indicated that maximum concentration of nickel is 13,48 mg·kg^{-1} in sample 10J while it is only around 1 mg·kg^{-1} for other gastropods.

Table 4.3 : Element concentrations of Gastropods (mg·kg^{-1}).

	Na	K	Cr	Fe	Co	Ni	Zn			
2014/10I	0.023	0.011	0.047	0.028	0.007	0.892	0.000			
2014/10J	0.026	0.011	0.009	0.019	0.185	13.485	0.000			
2014/10K	0.037	0.014	0.006	0.003	0.008	0.000	4.083			
2014/10P	0.019	0.000	0.004	0.002	0.012	1.863	0.000			
	Sc	As	Rb	Sr	Zr	Sb	Cs	Ba	Hf	Ta
2014/10I	0.002	0.123	0.000	2.649	0.000	0.006	0.000	0.270	0.000	0.000
2014/10J	0.005	0.004	0.000	1.990	0.097	0.030	0.000	0.195	0.000	0.000
2014/10K	0.002	0.008	0.000	3.034	0.062	0.000	0.000	0.173	0.000	0.000
2014/10P	0.005	0.004	0.000	1.807	0.000	0.000	0.000	0.166	0.000	0.000
	La	Ce	Nd	Sm	Eu	Tb	Yb	Lu	Th	U
2014/10I	1.732	0.162	0.207	1.200	0.165	0.123	0.067	0.124	0.006	0.000
2014/10J	0.921	1.161	1.695	0.623	0.892	0.411	0.144	0.068	0.073	0.130
2014/10K	1.053	0.702	1.044	0.660	0.511	0.235	0.085	0.081	0.023	0.091
2014/10P	0.710	0.695	0.634	0.456	0.332	0.167	0.077	0.119	0.026	0.035

It suggest that 10J was accumulated Ni up to 13 times higher than the others thus it can be a different type of gastropod. Similar pattern can be seen in sample 10K with its Zn concentration value being not only the highest, but also the only one which is in detection limits.

4.4   Elemental analysis of *Mytilus galloprovincialis*

Table 4.4 presents elemental concentrations of *Mytilus galloprovincialis*. The depth where *Mytilus galloprovincialis* was removed may play an important role on accumulated Sr levels, as can be seen from Table 4.4 and Table 3.1. The depth decreases from sample 10D to 10O as Sr increases and As behaves the opposite way. Also for sample 10N, there is a slight difference between U levels and other lanthanides.

Table 4.4 : Element concentrations of *Mytilus galloprovincialis* (mg·kg^{-1}).

	Na	K	Cr	Fe	Co	Ni	Zn			
2014/10A	0.206	0.000	0.007	0.014	0.089	2.149	0.000			
2014/10D	0.289	0.000	0.019	0.026	0.032	2.121	2.023			
2014/10N	0.315	0.000	0.000	0.002	0.004	0.905	0.000			
2014/10O	0.325	0.000	0.005	0.005	0.004	0.000	0.000			
	Sc	As	Rb	Sr	Zr	Sb	Cs	Ba	Hf	Ta
2014/10A	0.007	0.033	0.000	3.276	0.042	0.009	0.000	0.062	0.000	0.000
2014/10D	0.023	0.288	0.015	1.229	0.037	0.015	0.019	0.070	0.015	0.012
2014/10N	0.002	0.004	0.000	3.649	0.024	0.000	0.000	0.031	0.000	0.000
2014/10O	0.013	0.000	0.000	3.825	0.039	0.000	0.000	0.045	0.000	0.000
	La	Ce	Nd	Sm	Eu	Tb	Yb	Lu	Th	U
2014/10A	0.227	0.247	0.241	0.207	0.181	0.160	0.098	0.098	0.101	0.165
2014/10D	0.049	0.058	0.000	0.041	0.093	0.109	0.113	0.000	0.026	0.028
2014/10N	0.012	0.018	0.000	0.034	0.016	0.014	0.000	0.000	0.002	0.360
2014/10O	0.156	0.120	0.159	0.180	0.232	0.280	0.306	0.308	0.015	0.199

4.5   Elemental analysis of *Ostrea edulis*

Zinc was found to be the most abundant element in the investigated bivalve species, the highest being in oyster. It was reported that oysters are fine Zn accumulators. This element, which plays a role in the structure of the enzyme that is responsible for making one of the shells, is stored as a form of detoxified granules within the organism [30]. Results are being shown in Table 4.5, support this idea.

Table 4.5 : Element concentrations of *Ostrea edulis* (mg·kg⁻¹).

	Na	K	Cr	Fe	Co	Ni	Zn			
2014/10F	0.113	0.000	0.442	0.080	0.099	5.629	5.648			
2014/10L	0.375	0.051	0.005	0.007	0.044	3.300	3.430			
2014/10R	0.311	0.000	0.702	0.028	0.060	4.143	2.032			
	Sc	**As**	**Rb**	**Sr**	**Zr**	**Sb**	**Cs**	**Ba**	**Hf**	**Ta**
2014/10F	0.046	0.051	0.068	1.540	0.259	0.066	0.054	0.143	0.175	0.063
2014/10L	0.002	0.207	0.000	1.779	0.049	0.000	0.000	0.102	0.000	0.000
2014/10R	0.009	0.189	0.000	2.938	0.164	0.036	0.004	1.600	0.152	0.018
	La	**Ce**	**Nd**	**Sm**	**Eu**	**Tb**	**Yb**	**Lu**	**Th**	**U**
2014/10F	0.061	0.204	0.217	0.092	0.276	0.260	0.234	0.105	0.084	0.268
2014/10L	0.168	0.777	0.936	0.192	0.507	0.235	0.089	0.154	0.057	0.302
2014/10R	0.056	0.061	0.000	0.060	0.033	0.035	0.034	0.046	0.054	0.088

4.6 Elemental analysis of tortoise shell

Tortoise shells are composed of bone, and an incrementally grown covering of keratinized tissue (scutes) that can function as a repository for certain bioaccumulated trace elements. Since hard keratinized tissues of this type are virtually isolated from other metabolic activity, resident elemental species have limited mobility [12]. It is reasonable to assume therefore, that the grown shell of the tortoise represent a relatively stable elemental uptake. As shown in Table 4.6 most abundant elements in shell are Ni, Zn, and Lu. Similar results were obtained by fish vertebras (see also Table 4.2) consistent with its bone like chemical composition thus it may be evaluated alongside with fish vertebras.

Table 4.6 : Element concentrations of tortoise shell (mg·kg⁻¹).

|	Na	K	Cr	Fe	Co	Ni	Zn			
2014/10U(1)	0.217	0.000	0.080	1.070	0.820	30.56	52.89			
	Sc	**As**	**Rb**	**Sr**	**Zr**	**Sb**	**Cs**	**Ba**	**Hf**	**Ta**
2014/10U(1)	0.154	0.341	0.009	1.671	3.298	0.228	0.039	1.919	0.047	0.023
	La	**Ce**	**Nd**	**Sm**	**Eu**	**Tb**	**Yb**	**Lu**	**Th**	
2014/10U(1)	4.42	3.50	3.63	4.79	3.51	4.44	5.28	14.26	0.09	

4.7 Elemental analysis of non determined species

By comparing element concentration in Table 4.7 with the data obtained from the study it can be found a correlation between other species. In fact the element distributions are not only similar thoroughout the two samples, it is almost exactly proportional with from the *Acanthocardia spinosa* familia, namely 10M(2) (See Table 4.1 and Figure 4.1).

**Table 4.7 :** Element concentrations of non determined species (mg·kg^{-1}).

|	Na	K	Cr	Fe	Co	Ni	Zn		
2014/10C	0.159	0.016	0.006	0.005	0.008	0.000	0.000		
2014/10E	0.238	0.060	0.003	0.013	0.008	0.000	0.000		
	Sc	**As**	**Rb**	**Sr**	**Zr**	**Sb**	**Cs**	**Ba**	**Hf**	**Ta**
2014/10C	0.005	0.100	0.000	1.416	0.035	0.000	0.000	0.136	0.000	0.000
2014/10E	0.004	0.835	0.000	3.176	0.000	0.003	0.000	0.040	0.000	0.000
	La	**Ce**	**Nd**	**Sm**	**Eu**	**Tb**	**Yb**	**Lu**	**Th**	**U**
2014/10C	0.065	0.611	0.617	0.088	0.299	0.142	0.068	0.111	0.024	0.202
2014/10E	0.189	0.056	0.000	0.219	0.041	0.046	0.053	0.188	0.003	0.402
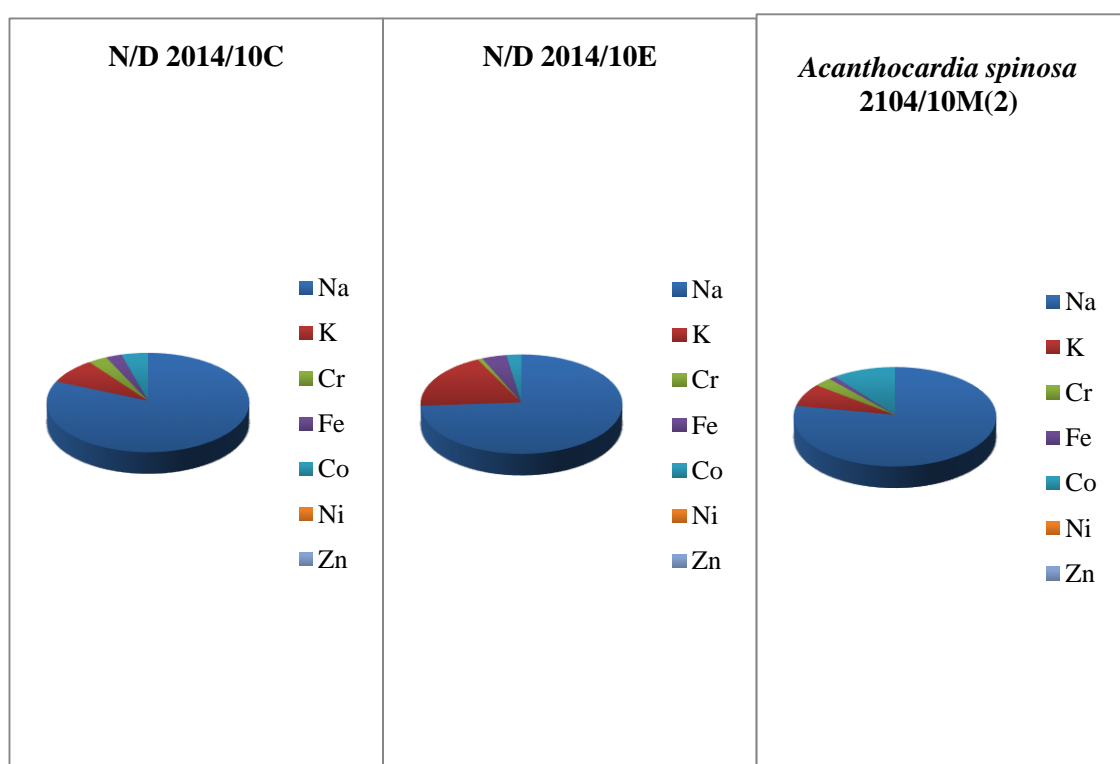
Figure 4.1 : Possible correlation between 10C, 10E and 10M(2).

4.8 Element fingerprints for investigated species

It is clear from the Figure 4.2 that, among essential elements detected in organisms, Zn and Ni have selective peak values for bones. Similar path is observed for the elements, which belong to the group of Lanthanides and Actinides, especially Th and U (see Figure 4.3).
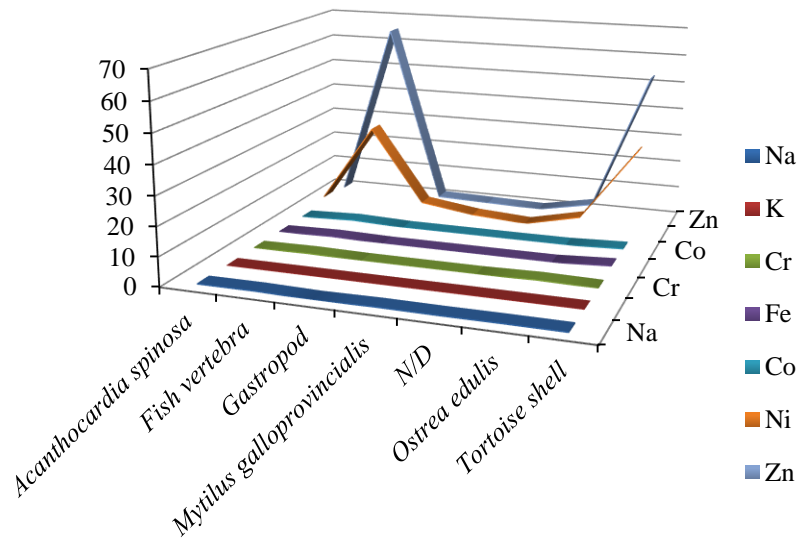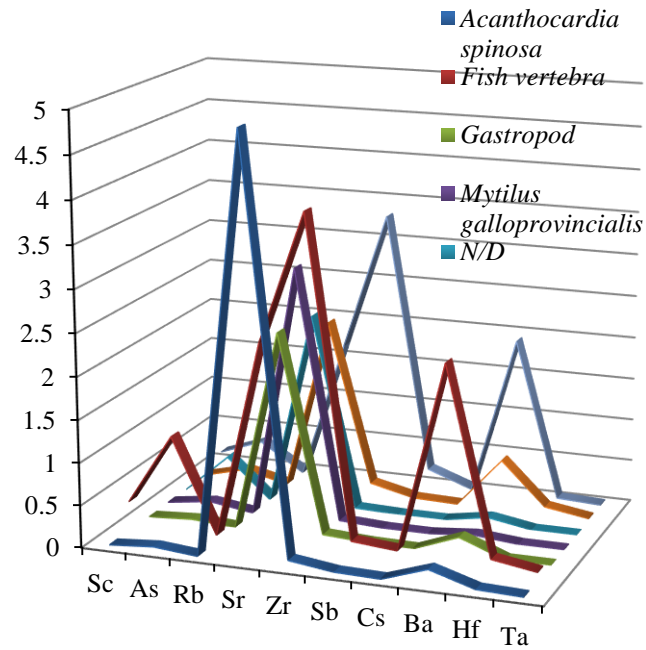
Figure 4.2 : Essential element distribution in samples according to average concentration values between species.
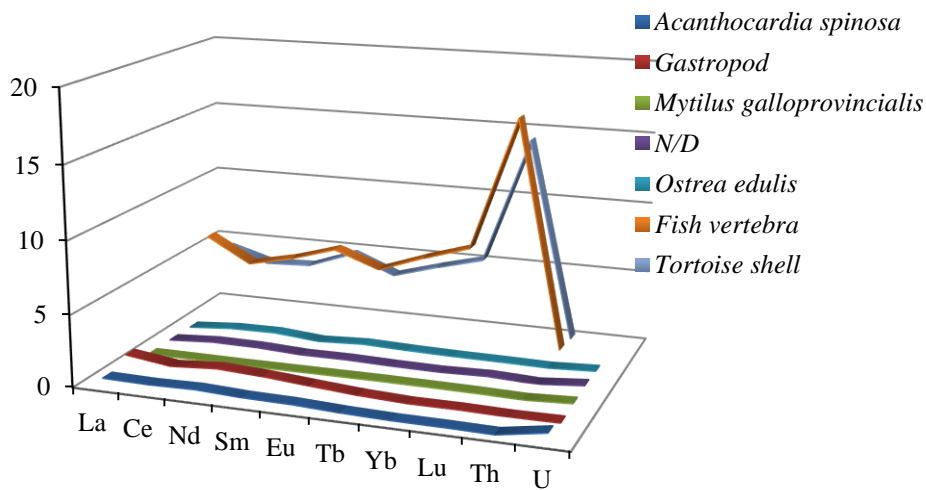

Figure 4.3 : Lanthanides and actinides element distribution in samples according to average concentration values between species.

As seen from Figure 4.4, Sr and Ba increase distinctly throughout species and can be further discussed regarding its function in living organisms or forming shells.

Figure 4.4 : Non-essential element distribution in samples according to average concentration values between species.

Also with the depth increase, there is a sudden rise in some elements (see Figure 4.5) which are lower until 8,8 m but that can be contributed by certain species, since most of the samples which were from such depths are bones.
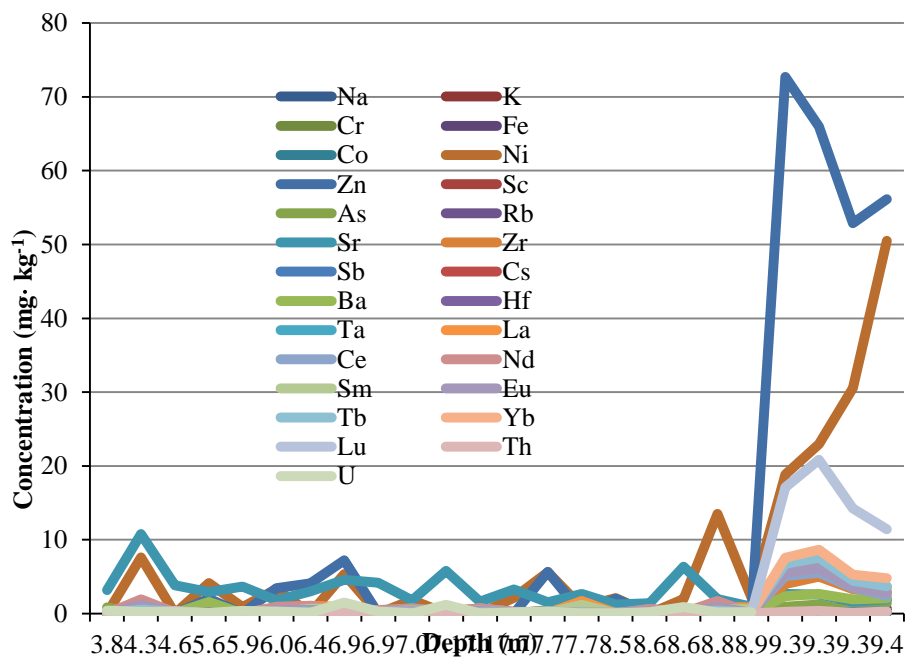

Figure 4.5 : Element concentrations according to depth.

5. CONCLUSION

In this study, more than 25 elements (As, Ba, Ce, Cs, Co, Cr, Eu, Fe, Hf, K, La, Lu, Na, Nd, Ni, Rb, Sb, Sc, Sr, Sm, Ta, Tb, Th, U, W, Yb, Zr and Zn) have been determined in archeological bones and shells in the interval of 0,0057-42350 mg·kg^{-1} by NAA. The results showed that reliable and representative results can be obtained from marine animals shells and bones.

The contents of some elements, especially La, Ce, Nd, Sm, Eu, Tb, Yb, Lu, Th, U in bones and tortoise shell reach very high values among other species where the maximum value of N/D sample reaching only 1,90 mg·kg^{-1}. Between bones and keratinized material, REEs and some other elements (As, Br) may migrate from soil into bones or untaken with the food products or resulted from the fission of uranium. It is also consistent with the depth increase and can be interpreted that the older the bone remains, the greater uranium content [31] (See Figure 5.1).
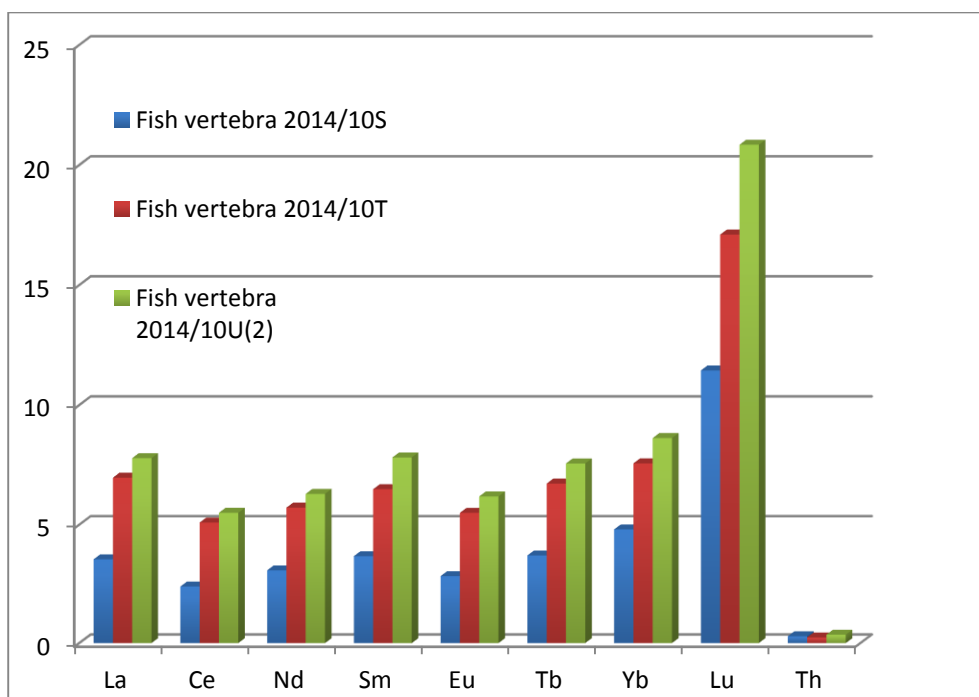

Figure 5.1 : Fish species lanthanide and actinide series distribution.

According to Chang et al. trace metal concentrations in shells of mollusk species vary to a wide range even if they belong to the same taxon. The differences between different species from different regions may be attributable to influential factors that govern the incorporation of trace metals during molluscan shell formation.

These influential factors can be summarized as differences in (a) taxonomies and ontogenetic stages, (b) mineralogy (biomineralization) of the shell, and (c) salinity and temperature of different water environments [32].

For bivalves it is known that the strength of the net accumulation patterns of metals vary both between metals but also, for one metal between species or more significantly between higher taxa such as families, correlating with their metal physiology including their ability to excrete or store particular trace elements. These factors explain the variation between, for example, the very high zinc concentrations in oysters (Ostreidae) and the much lower zinc concentrations in mussels (Mytilidae) [33] (See Figure 5.2).
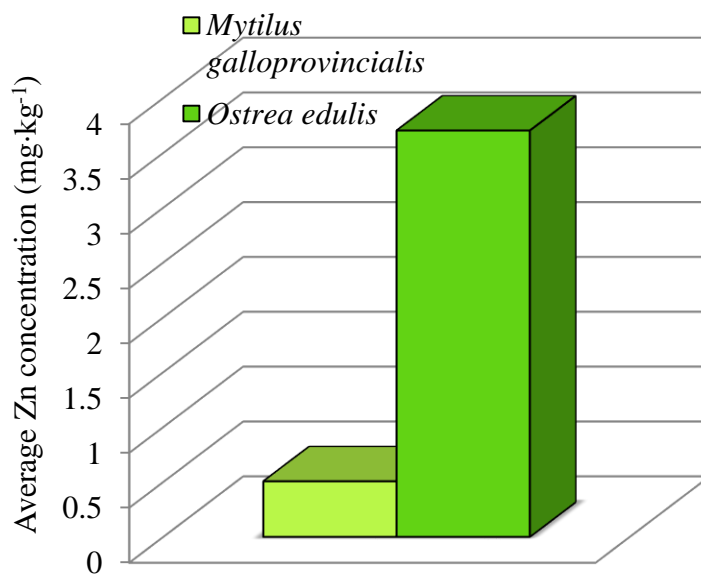
Figure 5.2 : Zn concentrations for *Mytilus g*. and *Ostrea e*. species (mg·kg^{-1}).

Such variation is expected in the Bivalvia where there are consistent differences in metal accumulation patterns between families including mytilids, ostreids, pectinids and venerids.

To conclude we can say considering that the organisms are the most active and deterministic factors of the environment, data obtained in this study will serve as a database for future studies.

REFERENCES

[1] **Marine and Commerce** (2012). Marmaray Project Reveals 8,500 Years Of Unknown History Of Istanbul, Marine and Commerce, ISSN: 1305-2918, March 2012 (pp. 34-36).

[2] **Greenberg R. R., Bode P., and De Nadai Fernandes E.** (2011). Neutron activation analysis: A primary method of measurement, Spectrochimica Acta Part B, Vol. 66, 193-241.

[3] **Gunay, E.** (2010). Qualitative and quantitative analysis of human hair with neutron activation analysis (M.Sc. Thesis). Retrieved from https://tez.yok.gov.tr/UlusalTezMerkezi/

[4] **Ohde S.** (1998). Determination of rare earth elements in recent and fossil shells by radiochemical neutron activation analysis. Journal of Radioanalytical and Nuclear Chemistry, Vol. 237, 51-54.

[5] **Celik A., Kaska Y., Bağ H., Aureggi M., Semiz G., Arslan Kartal A., and Elci L.** (2006). Heavy metal monitoring around the nesting environment of green sea turtles in Turkey. Water, Air, and Soil Pollution, Vol. 169, 67-79.

[6] **Glascock M. D. and Neff H.** (2003). Neutron activation analysis and provenance research in archaeology. Measurement Science and Technology, Vol. 14, 1516-1526.

[7] **Url-1** < *http://www.naa-online.net/theory/equations/*>, date retrieved 06.12.2014.

[8] **Haciyakupoglu S.** (2012). Radiometric Techniques In Environmental Analysis. ITU Radiation Science and Technologies Program, Environmental Trace Element Analysis Methods Course Notes 2.

[9] **Hamidatou L., Slamene H., Akhal T., and Zouranen B.** (2013). Imaging and Radioanalytical Techniques in Interdisciplinary Research - Fundamentals and Cutting Edge Applications, Chapter 6: Concepts, Instrumentation and Techniques of Neutron Activation Analysis, http://dx.doi.org/10.5772/53686.

[10] **Ciliberto E. and Spoto G.** (2000). Modern Analytical Methods in Art and Archaeology. Chemical Analysis: A Series Of Monographs On Analytical Chemistry And Its Applications, Vol. 155, pp. 81-127.

[11] **Nigra B. T., Faull K. F., and Barnard H.** (2014). Analytical Chemistry in Archaeological Research. Anal. Chem., doi:10.1021/ac5029616, American Chemical Society publications, Los Angeles.

[12] **Seltzer M. D., Berry K. H.** (2005). Laser ablation ICP-MS profiling and semiquantitative determination of trace element concentrations in

desert tortoise shells: documenting the uptake of elemental toxicants. Science of the Total Environment, Vol. 339, 253-265.

[13] **Nadkarni R. A. and Morrison G. H.** (1973). Multi element Instrumental Neutron Activation Analysis of Biological Materials. Analytical Chemistry, Vol. 45, No. 11 1957-1960.

[14] **Url-4** < *http://www2.kenes.com/stroke2014/info/Pages/AboutIstanbul.aspx>*, date retrieved 09.03.2015.

[15] **Yalcin M. N., Algan O., Ozdogan M., Yilmaz I., Sari E., Kirci-Elmas E., Bulkan O., Ongan D., Gazioglu C., Yilmaz Y., Nazik A., Polat M. A., and Meric E.** (2011). Holocene coastal change in the ancient harbor of Yenikapı–İstanbul and its impact on cultural history, Quaternary Research, Vol. 76, 30-45.

[16] **Buket Z., Belkaya H., Ozmen I. H., and Karamut I.** (2012). The Marmaray Project: Taking Good Care of the Natural Environment And The Historical Heritage Of Istanbul, http://www.ctta.org/fileupload/ita/2009/papers/p-10/p-10-03.pdf

[17] **Bony G., Marriner N., Morhange C., Kaniewski D., and Perinçek D.** (2012). A high-energy deposit in the Byzantine harbour of Yenikapı, Istanbul (Turkey), Quaternary International, Vol. 266, 117-130.

[18] **Algan O., Yalcin M. N., Ozdogan M., Yilmaz I., Sari E., Kirci-Elmas E., Ongan D., Bulkan-Yesiladalı B., Yilmaz Y., and Karamut I.** (2009). A short note on the geo-archeological significance of the ancient Theodosius harbor (İstanbul, Turkey), Quaternary Research, Vol. 72, 457-461.

[19] **Landmann G., Kempe S., Bichler M., Steinhauser, G., and Sterba H. J.** (2011). Geochemical fingerprints by activation analysis of tephra layers in Lake Van sediments, Turkey. Applied Radiation and Isotopes, Vol. 69, 929-935.

[20] **Url-2** < *http://www.tuwien.ac.at/dle/pr/aktuelles/downloads/2010/zehntausend ster_betriebstag_des_forschungsreaktors_am_atominstitut/>*, date retrieved 12.12.2014.

[21] **Taylor Ross S., and McLennan M. S.,** (1985). The Continental Crust: its Composition and Evolution, Blackwell Scientific Publications

[22] **Taylor S. R.** (1964). Abundance of chemical elements in the continental crust: a new table, Geochimica et Cosmochimica Acta, Vol. 28, 1273-1285.

[23] **Gromet L. P., Dymek R. F., Korotev R. L., and Haskin L. A.** (1984). The ''North American shale composite'': Its compilation major and trace element characteristics, Geochimica et Cosmochimica Acta, Vol. 48, 2469-2482.

[24] **Potts P. J. and Whitley J. E.** (1976). Determination and Interpretation of Rare-earth Abundances in Rocks and Minerals, Proc. Analysis Division Chem. Soc., 118-121

[25] **Peltz C., Schmid P., and Bichler M.** (1999). INAA of Aegaen pumices for the classification of archaeological findings, Journal of Radioanalytical and Nuclear Chemistry, Vol. 243, No. 2, 361-377.

[26]   **Url-3**   <
http://serc.carleton.edu/research_education/geochemsheets/technique s/INAA.html>, date retrieved 12.12.2014.

[27] **Bichler M., Steinhauser, G., and Sterba H. J.** (2007). ''Chemical fingerprints'' of pumice from Cappadocia (Turkey) and Kos (Greece) for archaeological applications. Applied Radiation and Isotopes, Vol. 65, 488-503.

[28] **Steinhauser, G., Sterba H. J., Bichler M., and Huber H.** (2006). Neutron activation analysis of Mediterranean volcanic rocks− An analytical database for archaeological stratigraphy. Applied Geochemistry, Vol. 21, 1362-1375.

[29] **Yamada M., Fujimori K., Yamada G., Moriwake Y., Tohno S., and Tohno Y.** (2001). Trace Metals in Vertebral Columns of Deep-Sea Teleost Fish. Biological Trace Element Research, Vol. 80, 245-249.

[30] **Colakoglu S., Ulukoy G., Ormanci H.B., and Colakoglu F. A.** (2012). Metal levels in economically important bivalve species from Turkey, Food Additives & Contaminants: Part B: Surveillance, 5:4, 272-278, DOI: 10.1080/19393210.2012.707233

[31] **Vasidov A., Osinskaya N. S., Khatamov Sh., Rakhmanova T., and Akhmadshaev A. Sh.** (2008). Instrumental neutron activation analysis of prehistoric and ancient bone remains. Journal of Radioanalytical and Nuclear Chemistry, Vol. 278, No.2, 287-291.

[32] **Pourang N., Richardson C. A., Chenery S. R. N. and Nasrollahzedeh H.** (2014). Assessment of trace elements in the shell layers and soft tissues of the pearl oyster Pinctada radiata using multivariate analyses: a potential proxy for temporal and spatial variations of trace elements. Environmental Monitoring Assessment, Vol. 186, 2465-2485.

[33] **Marsden I. D., Smith B. D., Rainbowb P. S.** (2014). Effects of environmental and physiological variables on the accumulated concentrations of trace metals in the New Zealand cockle Austrovenus stutchburyi. Science of the Total Environment Vol. 470–471, 324–339.

CURRICULUM VITAE

Name Surname:	**Ayşe Tuba ÖNGÜL**
Place and Date of Birth:	**Istanbul 12.02.1987**
Address:	**Çaldıran Sk. Akmara Apt. 16/10 Bahçelievler/Istanbul**
E-Mail:	**aongul@itu.edu.tr**
B.Sc.:	**Yildiz Technical University – Physics 2011**